Pa. 242

ANL-78-21

182
7-11-78

HIGH-PERFORMANCE BATTERIES FOR STATIONARY ENERGY STORAGE AND ELECTRIC-VEHICLE PROPULSION

Progress Report for the Period October–December 1977

MASTER

ARGONNE NATIONAL LABORATORY, ARGONNE, ILLINOIS

Prepared for the U. S. DEPARTMENT OF ENERGY
under Contract W-31-109-Eng-38

DISTRIBUTION OF THIS DOCUMENT IS UNLIMITED

The facilities of Argonne National Laboratory are owned by the United States Government. Under the terms of a contract (W-31-109-Eng-38) between the U. S. Department of Energy, Argonne Universities Association and The University of Chicago, the University employs the staff and operates the Laboratory in accordance with policies and programs formulated, approved and reviewed by the Association.

MEMBERS OF ARGONNE UNIVERSITIES ASSOCIATION

The University of Arizona
Carnegie-Mellon University
Case Western Reserve University
The University of Chicago
University of Cincinnati
Illinois Institute of Technology
University of Illinois
Indiana University
Iowa State University
The University of Iowa
Kansas State University
The University of Kansas
Loyola University
Marquette University
Michigan State University
The University of Michigan
University of Minnesota
University of Missouri
Northwestern University
University of Notre Dame
The Ohio State University
Ohio University
The Pennsylvania State University
Purdue University
Saint Louis University
Southern Illinois University
The University of Texas at Austin
Washington University
Wayne State University
The University of Wisconsin

NOTICE

This report was prepared as an account of work sponsored by the United States Government. Neither the United States nor the United States Department of Energy, nor any of their employees, nor any of their contractors, subcontractors, or their employees, makes any warranty, express or implied, or assumes any legal liability or responsibility for the accuracy, completeness or usefulness of any information, apparatus, product or process disclosed, or represents that its use would not infringe privately-owned rights. Mention of commercial products, their manufacturers, or their suppliers in this publication does not imply or connote approval or disapproval of the product by Argonne National Laboratory or the U. S. Department of Energy.

Printed in the United States of America
Available from
National Technical Information Service
U. S. Department of Commerce
5285 Port Royal Road
Springfield, Virginia 22161
Price: Printed Copy $6.00; Microfiche $3.00

[illegible]
Energy Storage Electrochemical
(EC-76-C-)

ANL-78-21

Argonne National Laboratory
9700 South Cass Avenue
Argonne, Illinois 60439

HIGH-PERFORMANCE BATTERIES FOR STATIONARY ENERGY STORAGE AND ELECTRIC-VEHICLE PROPULSION

Progress Report for the Period
October—December 1977

P. A. Nelson	Director, Energy Storage
R. K. Steunenberg	Manager, Lithium/Metal Sulfide Battery Program
A. A. Chilenskas	Manager, Battery Commercialization
E. C. Gay	Section Manager, Battery Engineering
J. E. Battles	Group Leader, Materials Development
F. Hornstra	Group Leader, Battery Charging Systems
W. E. Miller	Group Leader, Industrial Cell and Battery Testing
M. F. Roche	Group Leader, Cell Chemistry
H. Shimotake	Group Leader, Cell Development and Engineering

March 1978

Previous Reports in this Series

ANL-77-17	October—December 1976
ANL-77-35	January—March 1977
ANL-77-68	April—June 1977
ANL-77-75	July—September 1977

PREFACE

The program on high-temperature secondary batteries at Argonne National Laboratory consists of an in-house research and development effort and subcontracted work by industrial laboratories. The work at Argonne is carried out primarily in the Chemical Engineering Division, with assistance on specific problems being given by the Materials Science Division and, from time to time, by other Argonne divisions. The individual efforts of many scientists, engineers, and technicians are essential to the success of the program, and recognition of these efforts is reflected by the individual contributions cited throughout the report.

TABLE OF CONTENTS

TABLE OF CONTENTS (Cont'd)

TABLE OF CONTENTS (Cont'd)

LIST OF FIGURES

LIST OF TABLES

HIGH-PERFORMANCE BATTERIES FOR STATIONARY ENERGY STORAGE AND ELECTRIC-VEHICLE PROPULSION

Progress Report for the Period
October—December 1977

ABSTRACT

This report describes the research, development, and management activities of the program at Argonne National Laboratory (ANL) on lithium/metal sulfide batteries during the period October-December 1977. These batteries are being developed for electric-vehicle propulsion and stationary energy storage. The present cells, which operate at 400-500°C, are of a vertically oriented, prismatic design with a central positive electrode of metal sulfide (usually, FeS or FeS_2), two facing negative electrodes of lithium-aluminum alloy, and an electrolyte of molten LiCl-KCl.

A major objective of this program is to transfer the technology to industry as it is developed, with the ultimate goal of a competitive, self-sustaining industry for the commercial production of lithium/metal sulfide batteries. Technology transfer is being implemented by several means, including the assignment of industrial participants to ANL for various periods of time and the subcontracting of development and fabrication work on cells, cell components, and battery testing equipment to industrial firms.

Testing and evaluation of industrially fabricated cells at ANL and industrial laboratories is continuing. These tests provide information on the effects of design modifications and alternative materials for cells. Improved electrode and cell designs are being developed and tested at ANL, and the more promising designs are incorporated into the industrially fabricated cells. Among the concepts receiving attention are carbon-bonded positive electrodes, pellet-grid electrodes, alternative materials for positive electrodes, additives to extend electrode lifetime, and alternative electrode separators.

Materials development efforts include the development and testing of materials for cell components; post-test examinations of cells were made to evaluate the behavior of cell materials and to determine the causes of cell failure. Chemistry studies were concerned primarily with the electrochemistry of FeS_2 and FeS electrodes. In studies of advanced battery systems, the use of calcium and magnesium alloys for the negative electrode is being investigated.

SUMMARY

Commercial Development

Studies are now being conducted on design features that may make the lithium/metal sulfide batteries superior to other types of batteries for near-term market applications (postal vans, buses, mining vehicles, and submarines). For example, the non-gassing characteristic of the Li-Al/FeS_x battery permits it to be hermetically sealed, thereby minimizing the possibility of explosion. This feature is particularly important for submarine and mining applications.

An update and refinement of a manufacturing cost study completed in 1976 has been initiated. This cost update will examine the cost for recently designed Li-Al/FeS and Li-Al/FeS_2 cells that have been fabricated by cost-effective techniques.

A cooperative effort between ANL and the Atomics International Division of Rockwell International leading to the design of a 5.6-MW-hr battery module for stationary energy storage has been initiated. Testing of a battery module in the BEST (Battery Energy Storage Test) Facility is expected to take place in 1983. A conceptual design of a prismatically shaped jacket for a 40-kW-hr electric-vehicle battery (Mark IA) is in progress.

Industrial Cell and Battery Testing

Eagle-Picher Industries, Inc. has fabricated most of the FeS and FeS_2 cells in their current contract with ANL. A review of the performance data of the cells that had been previously qualification tested has led to the following generalizations: utilization increases as electrolyte volume increases (constant electrode thickness), utilization increases as electrode thickness decreases (constant electrolyte volume), and specific energy of a cell is affected more by the capacity loading than by the utilization.

Other tests were conducted with Eagle-Picher cells to determine the effect on performance of charging current, operating temperature, and negative-to-positive capacity ratio. An FeS cell was cycled at charge-discharge currents of 10, 15, 20, and 25 A during 562 cycles of operation. The cell capacity was very stable at all four charge-discharge currents. Thermal tests that were conducted on three Li-Al/FeS cells have shown that their performance increases when the temperature is raised from 425 to 500°C, and that it returns to the original level when the temperature is returned to 425°C. Finally, preliminary results indicate that a cell with a negative-to-positive capacity ratio of 2:1 has slightly better performance than one with a ratio of 1:2.

Gould Inc. has fabricated 32 upper-plateau FeS_2 cells under their current subcontract with ANL. These cells are being tested to determine the effect on performance of (1) current-collector design, (2) lithium content in the negative electrode, (3) electrolyte volume and thickness of the positive electrode, and (4) method of particle retention. Preliminary testing on four of these cells has indicated that the utilization of active material is higher when the negative electrode contains 20.5 wt % rather than 17.5 wt % lithium.

At Atomics International, a 2.5 kW-hr Li-Si/FeS cell has been fabricated. This cell, which has 23 x 23 cm electrodes, is a major step in their development of stationary-energy-storage cells for the BEST Facility. The ANL subcontract with Atomics International also includes the development of FeS electrodes, powder separators, and Li-Si/FeS cells for electric vehicles.

Proposals were solicited for the development, design, and fabrication of a 40 kW-hr battery to be tested in an electric van at ANL early in 1979. Preparations are now under way for in-vehicle testing of lithium/metal sulfide batteries. The main tasks that are being addressed include on-board instrumentation for evaluation of battery performance and design of a battery charger.

A facility for testing up to 100 industrial cells is presently being built in CEN; to be included as an integral part of this facility is a computerized data-acquisition system. A facility is also being constructed for laboratory tests of electric-vehicle batteries that will precede in-vehicle tests. This facility will have the capability for computer-controlled operation and data-acquisition.

Cell Development and Engineering

Nickel sulfide is continuing to be explored as a substitute for the active material in the positive electrode or as an additive in Li-Al/MS_2 cells. Although Li-Al/NiS_2 cells had lower specific energies than Li-Al/FeS_2 cells, they did operate for relatively long periods of time (about 200 cycles) with little decline in capacity. A highly compact cell with a positive electrode containing 69 mol % $FeS_{1.46}$-31 mol % $NiS_{1.46}$ attained a high specific energy, 90 W-hr/kg at the 5-hr rate. Capacity of this cell has been very stable over its 170 cycles of operation. A carbon-bonded NiS_2 cell has also achieved a high specific energy, 81 W-hr/kg at the 4-hr rate. This cell has operated for over 100 cycles with stable capacity; the coulombic efficiency is 99.5%.

Experiments on small-scale cells are being undertaken to further define the optimum conditions for the preparation and operation of FeS electrodes. The operating temperature was raised from 450 to 500°C on two Li-Al/FeS cells and a Li-Al/$Ni_{0.5}Fe_{0.5}S$ cell. All three cells showed significant improvement in utilization (about 30%) at the higher operating temperatures. The use of LiCl-rich electrolyte in FeS cells operated at 450°C also increased the utilization by about 30%.

Studies are continuing on Li-Al/FeS cells with powder separators. An engineering-scale FeS cell with a MgO powder separator has operated for 97 cycles (70 days) without any loss in coulombic efficiency.

Materials Development

Efforts are continuing on the evaluation of candidates for electrode separators. Cell SC-25 was built with recently received BN felt and placed in operation. So far this cell has demonstrated the best performance among the Li-Al/FeS cells operated at ANL with BN felt separators. A test of

Cell SC-21, which had a MgO powder separator, was terminated after 80 days and 131 cycles of operation. The gradual decline in cell performance appears to have occurred as a result of extrusion of positive material through the thinner areas of the powder separator layer.

Flowability (creep) experiments on two powder separators and two powder separator-electrode material composites have been completed. The results indicate that a hot-pressed separator of MgO powder in an FeS cell should retain its shape after an initial movement among the particles, and that FeS particles will extrude into any free spaces under compressive stresses as low as 700 kPa.

Porous Y_2O_3 separator plates have been fabricated by the yttria-nitric acid plaster technique. A fabrication procedure has been developed that yields plates of reproducible quality. Warping of plates during firing is a problem that requires further study. Several electrically conductive ceramics (TiN and TiB_2) have been identified as potential coating materials for inexpensive current collectors. This type of current collector is being evaluated as a replacement for the expensive molybdenum current collectors presently used in FeS_2-type cells.

Experiments are being conducted on the vibratory loading of active material into porous metal structures. Aluminum powder was vibratorily loaded into Retimet structures to packing densities of 34-53 vol %. The packing densities were dependent on particle size distribution, Retimet pore size, and form (dry or slurry) of the aluminum powder. Future work will be aimed at achieving aluminum powder densities of 65-70 vol % in porous metal. Methods for retaining the particles after they are loaded will also be studied.

Contact-angle measurements were made on electrode materials to supplement previous data on separators and particle retainers. On surfaces of FeS_2, Fe and Li_2S, molten electrolyte was found to have an advancing contact angle that is nonwetting and a receding contact angle that is wetting. On a LiAl surface, the electrolyte spreads easily. Wetting of a positive electrode by electrolyte is expected to require the application of force, such as evacuation and repressurization of the cell atmosphere.

A new method of pretreating BN felt ("dusting" with $LiAlCl_4$) has been tested and found to be effective in producing a separator surface that is easily wet by molten electrolyte. In addition, equipment has been fabricated for the wetting of BN separators with molten electrolyte before cell assembly. Several separators will be prepared to test this prewetting procedure.

Post-test examinations were continued on vertical, prismatic engineering cells and on small-scale laboratory cells. Carbon analyses of negative electrodes from cells having positive electrodes that were carbon-bonded or contained added carbon indicated a significant migration of the carbon to the negative electrode. The amount of carbon migration is suspected to depend on cell lifetime and the quantity of carbon added to the positive electrode. Examination of Y_2O_3 separators from FeS and FeS_2 cells has shown evidence of sulfur reaction with the Y_2O_3 to form Y_2O_2S. These studies indicate that

Y_2O_3 may not be a satisfactory separator material. Metallographic and chemical analyses previously indicated a significant lithium concentration gradient in charged Li-Al electrodes; this was further confirmed by ion microprobe analyses on three cells.

Twenty vertical, prismatic engineering cells underwent post-test examination to determine the causes of cell failure. The major cause of failure was the cutting of cell separators by the honeycomb current collector of the positive electrode. These cells were fabricated prior to the recommendation to add protective screens.

Cell Chemistry

The current status of the Li-Fe-S phase diagram is presented. The important phases are FeS_2, $Fe_{1-x}S$, $Li_3Fe_2S_4$, Li_2FeS_2, Fe, and a solid solution that is connected with Li_2FeS_2 and is rich in sulfur. This phase diagram was used to describe the discharge-charge mechanism of the FeS_2 electrode in LiCl-KCl electrolyte.

Studies were conducted on the behavior of FeS_2 electrodes in LiCl-KCl electrolyte of varying composition (eutectic, KCl-rich, and LiCl-rich). Cyclic voltammetry studies, cell tests, and metallographic studies showed that $KFeS_2$ formed during the charging of FeS_2 electrodes in KCl-rich electrolyte. Cyclic voltammetry studies also showed that electrochemical irreversibility of FeS_2 electrodes in LiCl-rich and eutectic electrolyte is caused by products that exist between 37.5% and 50% discharge.

Metallographic studies were performed on the use of CoS_2 as an additive to FeS_2 electrodes. These studies indicated that Li-Co-S analogs of Li-Fe-S compounds do not exist at cell operating temperature. Thus cobalt and iron sulfides follow independent charge-discharge paths, with cobalt present as its binary Co-S compounds. It was recommended that a reassessment of the effects of this additive on cell performance should be undertaken.

Cell tests and voltammetry studies that were performed on Li-Al/FeS cells confirmed earlier studies which had indicated that the conversion of $LiK_6Fe_{24}S_{26}Cl$ (J phase) to FeS requires a potential of about 1.6 V *vs.* LiAl at 430°C. In tests on small-scale Li-Al/$Fe_{0.5}Ni_{0.5}S$ cells, J phase, probably with nickel substituted for a portion of the iron, was found. In tests on small-scale Li-Al/FeSe cells, a selenium analog of J phase was found.

Studies of the properties of lithium negative electrodes were also undertaken. A lithium wick/NiS cell was operated; positive electrode swelling caused cell failure after 11 cycles. Operation of Li-Al electrodes containing various additives (In, Sn, Pb, Cu, Ag, Sb, Zn, or Mg) showed that indium is the only one of the above additives that significantly improves capacity retention.

Advanced Battery Research

The objective of this program is to devise new combinations of electrode materials and electrolytes that will provide a basis for the development of inexpensive, high-performance batteries.

A $CaAl_2$ (17 A-hr)/LiCl-KCl-$CaCl_2$/NiS_2 (4.7 A-hr) cell was operated at 442°C. Carbon powder (14 wt %) was added to the positive electrode. This cell achieved a higher utilization (72% at 27 mA/cm^2 to 50% at 80 mA/cm^2) than a similar cell which had cobalt as the positive electrode additive.

A 70 A-hr sealed, prismatic Ca(Mg_2Si)/NiS_2 cell (composition at full charge) has been placed in operation to evaluate the behavior of the calcium electrode in a practical configuration. The cell was assembled in the uncharged condition, and no calcium metal was used in its fabrication. During the first 30 cycles of operation, this cell has achieved a specific energy of 42 W-hr/kg at the 6-hr rate. This specific energy is 70% of the demonstration goal.

Studies of magnesium cells included tests of Mg-Pb negative electrodes (theoretical capacity, 12 A-hr) as well as small-scale Mg_2Al_3/TiS_2 and Mg_2Al_3/NiS_2 cells. After operation of the Mg-Pb electrodes, examination showed that a short circuit was caused by growth of magnesium dendrites through the BN fabric separator. Both the Mg_2Al_3/TiS_2 cell and the Mg_2Al_3/NiS_2 cell exhibited poor utilization of the positive electrode at high current densities. Methods of circumventing the problems of dendrite formation and low positive-electrode utilization in magnesium cells will be investigated.

I. INTRODUCTION

Lithium/metal sulfide batteries are being developed at Argonne National Laboratory (ANL) for use as (1) power sources for electric vehicles, and (2) stationary-energy-storage devices for load-leveling on electric utility systems or storage of electrical energy produced by solar, wind, or other sources. The performance and lifetime goals that are projected for prototypes of electric-vehicle and stationary-energy-storage batteries in 1985 are presented in Table I-1. Future revisions of these goals may become appropriate as the requirements of these two applications are defined more specifically by systems design studies.

Table I-1. Performance Goals for Lithium/Metal Sulfide Batteries

Battery Goals	Electric Vehicle Propulsion	Stationary Energy Storage
Power		
Peak	60 kW	25 MW
Sustained Discharge	25 kW	10 MW
Energy Output	45 kW-hr	100 MW-hr
Specific Energy,[a] W-hr/kg	180	60-150
Discharge Time, hr	4	5-10
Charge Time, hr	5-8	10
Cycle Life	1000	3000
Cost of Cells, $/kW-hr	35	20

[a]Includes cell weight only; the insulation and supporting structure is about 15 to 20% of the total weight for the electric-vehicle battery.

The strategy for the development of electric-vehicle batteries involves the development, design, and fabrication of a series of lithium/metal sulfide batteries by industrial subcontractors. Each of the batteries in this series, designated Mark I, II, and III, has a different set of objectives. The primary objective of the Mark I battery is to establish the technical feasibility of the lithium/metal sulfide system for electric-vehicle propulsion and to resolve any interfacing problems with the battery, the motors and controls, the vehicle itself, and the charger. The first in-vehicle test of a Mark I battery is currently scheduled for early in 1979. The Mark II battery has higher performance goals than Mark I, but the main emphasis is on the development of designs and materials that will permit low-cost manufacturing techniques, and the development of pilot-scale fabrication methods. The Mark III battery is planned as a high-performance prototype suitable for demonstration and evaluation in an electric automobile in 1983. Program goals for the Mark I, II, and III electric-vehicle batteries are listed in Table I-2.

Table I-2. Program Goals for the Mark I, II, and III Electric-Vehicle Batteries

	Mark I	Mark II	Mark III
Specific Energy, W-hr/kg			
Cell (average)	100	125	160
Battery	75	100	130
Energy Density, W-hr/liter			
Cell (average)	320	400	525
Battery	100	200	300
Peak Power, W/kg			
Cell (average)	100	125	200
Battery	75	100	160
Jacket Heat Loss, W	300	150	125
Lifetime			
Deep Discharges[a]	400	500	1,000
Target Date	1979	1981	1983

[a]Utilization of more than 50% of the theoretical capacity every 10 cycles.

A decision was made in August 1977 to proceed with the procurement of the first Mark I battery, which is designated Mark IA, and a request for proposals was issued on November 2. The statement of work calls for a 40 kW-hr battery package consisting of two 20 kW-hr modules, which will be fabricated and delivered to ANL in 12 months. The battery cells are expected to be a multiple-electrode design employing Li-Al or Li-Si negative electrodes and FeS positive electrodes with molten LiCl-KCl eletrolyte.

Assessment studies have indicated that stationary-energy-storage batteries having a life of 8 to 12 years and a capital cost of about $20 to 30/kW-hr would be competitive with alternative methods of storing energy or producing supplemental power during peak demand periods. These long-lifetime and low-cost requirements are offset somewhat by the fact that the specific-energy and specific-power requirements are relatively modest. The cells currently being developed for stationary-energy-storage batteries have lithium-silicon or lithium-aluminum electrodes. A conceptual design by ANL involves a multiple-electrode cell configured as a cube about 25 cm on an edge, with a capacity of 4.4 kW-hr. The Atomics International Division of Rockwell International* has developed a somewhat similar conceptual design for a stationary-energy-storage cell. A common conceptual design for a battery module based on these cell designs is being developed as a joint effort between Atomics International and ANL; this module will serve as the basis for

*Under contract with ANL.

a design of a utility storage plant having a capacity of 100 MW-hr. The experimental portion of this effort will involve the development of a 5-6 MW-hr module that will be tested in the BEST (Battery Energy Storage Test) Facility.

The lithium/metal sulfide battery program consists of an in-house research and development effort at ANL and subcontracts with several industrial firms. The major industrial subcontractors are Atomics International, Carborundum Co., Catalyst Research Corp., Eagle-Picher Industries, Inc., and Gould Inc. The ANL effort includes cell chemistry studies, materials development and evaluation, cell and battery development, industrial cell and battery testing, and commercialization studies. Preparations are also being made for in-vehicle tests of the Mark IA battery and for statistical lifetime testing of cells. Another small effort at ANL is directed toward the development of advanced battery systems that use low-cost, abundant materials.

Figures I-1 to I-6 illustrate the improvements in lifetime and performance of Li-Al/FeS and Li-Al/FeS_2 cells that have taken place during the past few years. The M-, R-, KK- and CB-series cells were designed and fabricated at ANL; the others were built by industrial subcontractors. Also shown in these figures are performance and lifetime goals for the cells of electric-vehicle batteries. In general, the Li-Al/FeS cells have shown long cycle life (Fig. I-3), but they are limited in specific energy (Fig. I-1) and specific power (Fig. I-2). The specific energy is expected to be significantly higher for multiplate cells than for the bicells that were tested. A similar gain in the specific power is anticipated. The Li-Al/FeS_2 cells have achieved higher specific energy (Fig. I-4) and power (Fig. I-5) than the FeS cells, but the cycle life (Fig. I-6) has not exceeded about 500 cycles for the cells tested to date.

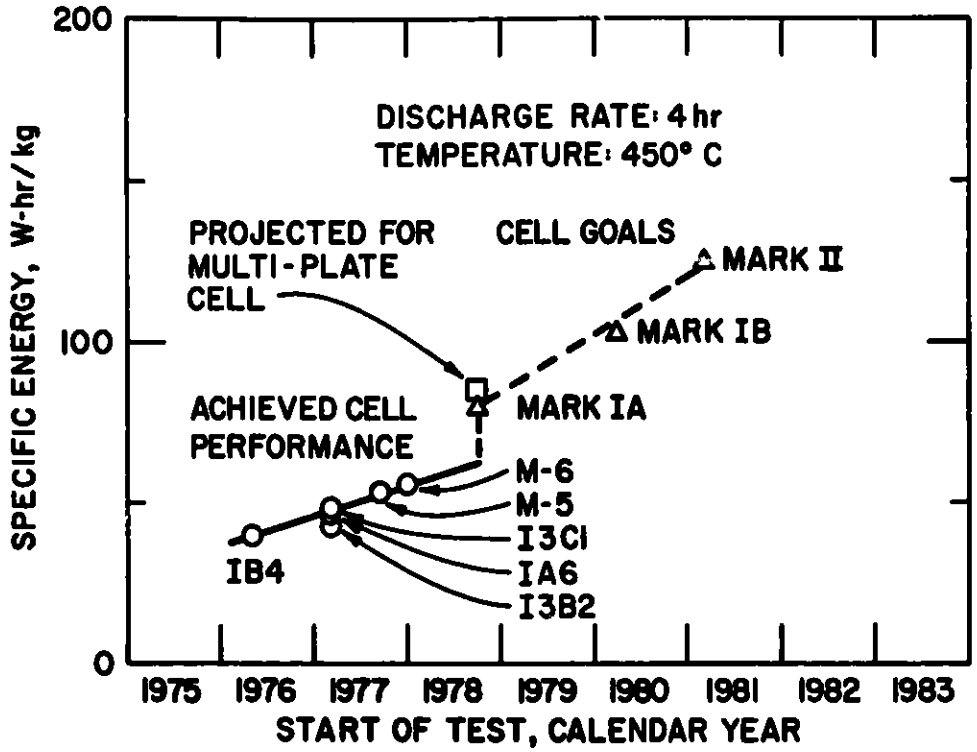

Fig. I-1. Specific Energy of Li-Al/FeS Cells.
ANL Neg. No. 308-78-169

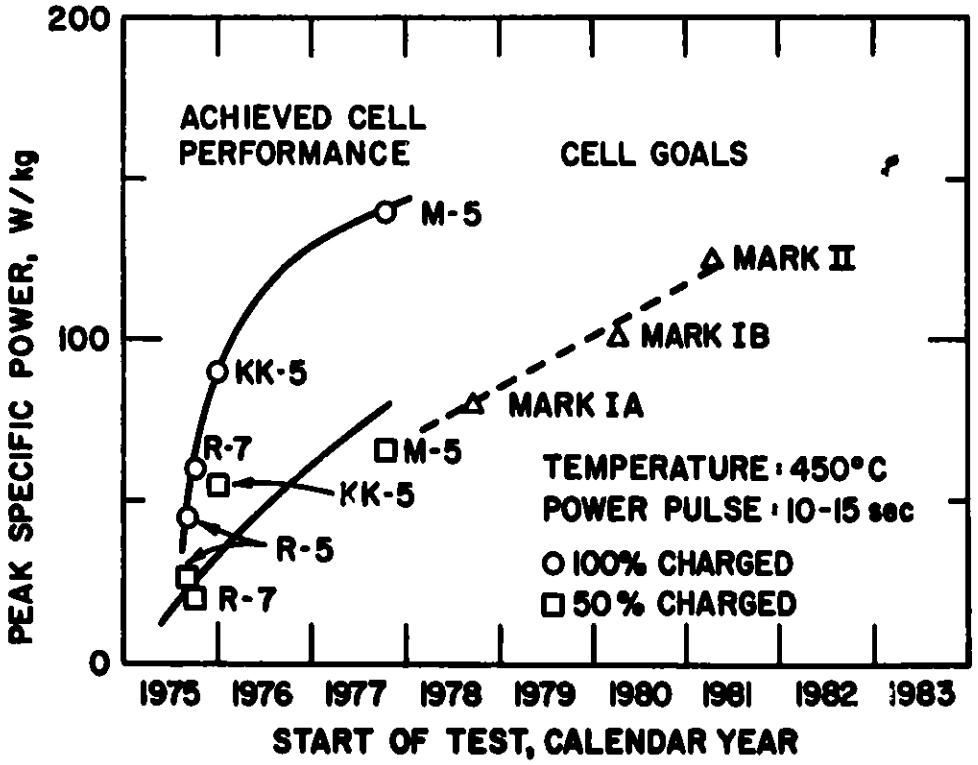

Fig. I-2. Peak Specific Power of Li-Al/FeS Cells.
ANL Neg No. 308-78-176

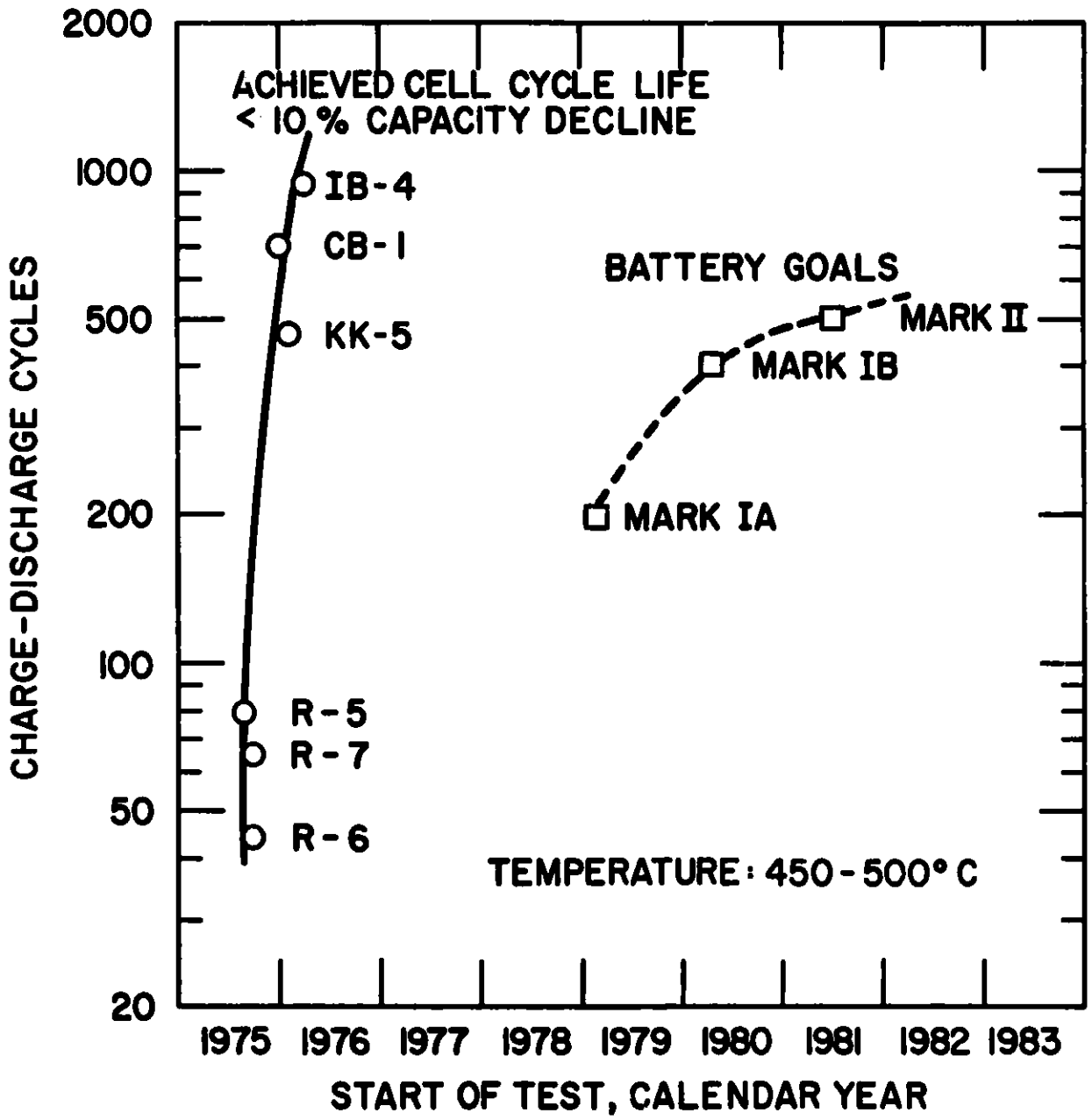

Fig. I-3. Cycle Life of Li-Al/FeS Cells.
ANL Neg. No. 308-78-174

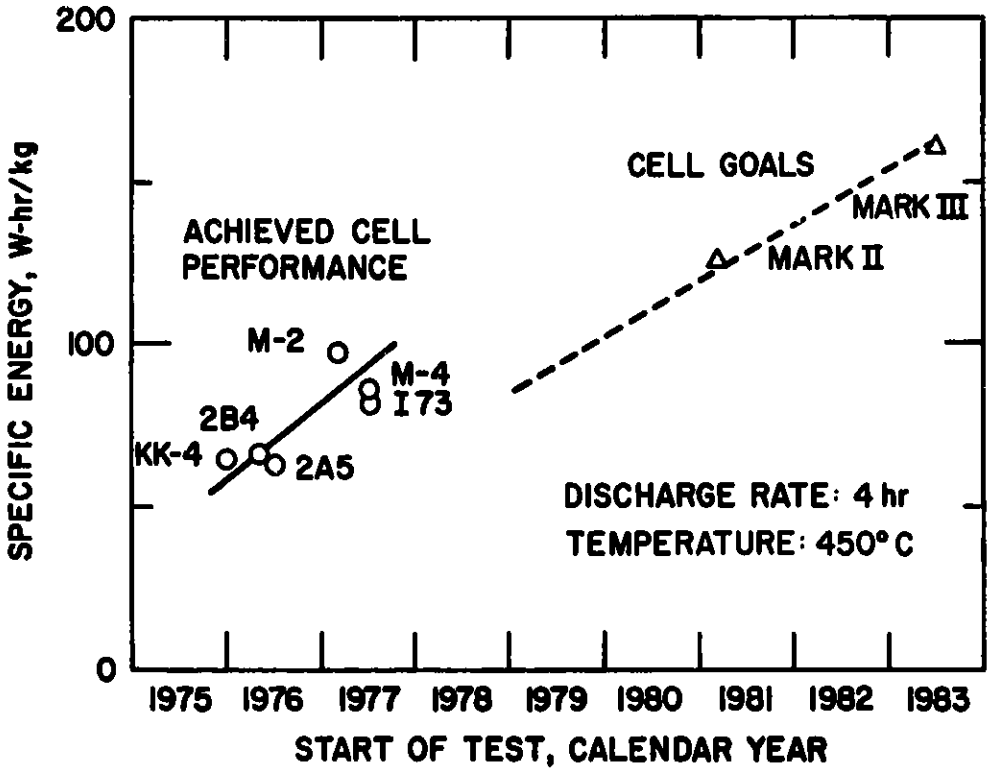

Fig. I-4. Specific Energy of Li-Al/FeS_2 Cells.
ANL Neg. No. 308-78-175

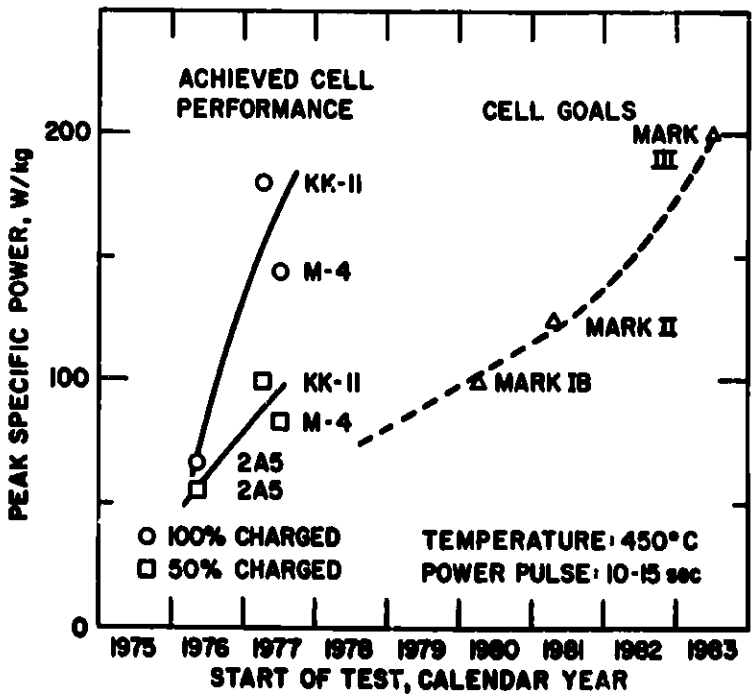

Fig. I-5. Peak Specific Power of Li-Al/FeS_2 Cells.
ANL Neg. No. 308-78-170

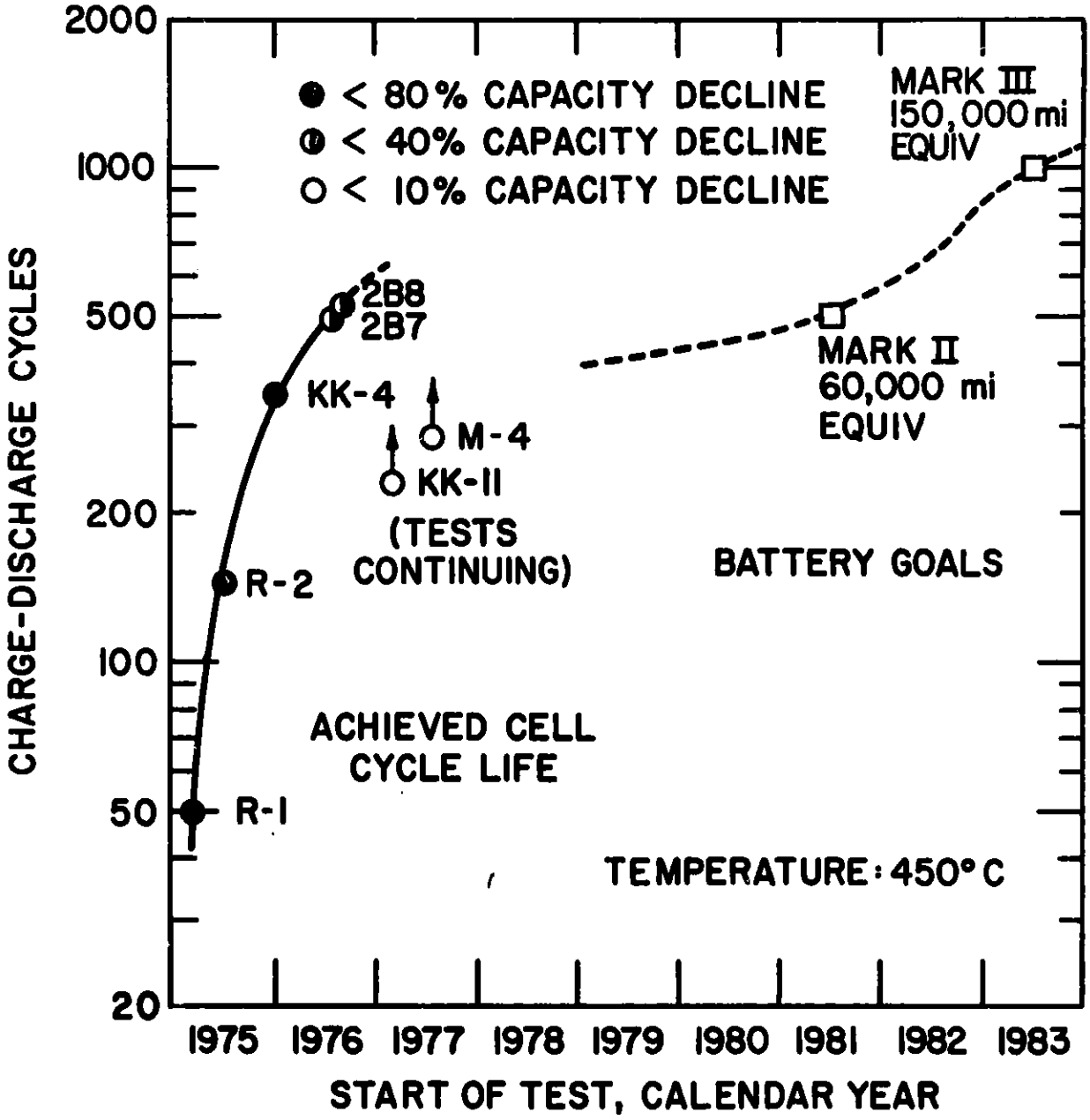

Fig. I-6. Cycle Life of Li-Al/FeS_2 Cells.
ANL Neg. No. 308-78-173

II. COMMERCIAL DEVELOPMENT
(A. A. Chilenskas)

Commercialization studies are conducted at ANL with assistance from industrial subcontractors and consultants. These studies involve the identification of potential markets, cost analyses, manufacturing and financial plans, and evaluations of competing technologies.

A. Commercialization Studies
(A. A. Chilenskas, W. H. Towle,* J. Graae,* W. R. Frost, J. E. Battles)

The first commercial production of the lithium/metal sulfide battery will probably be for limited markets such as postal vans, buses, mining vehicles, and submarines. An estimate of the size of these near-term markets is presented in ANL-77-68, pp. 10-13. In these near-term markets the relatively high price of the battery should be offset by its favorable performance characteristics. Studies are now being conducted on design features that may make the lithium/metal sulfide batteries superior to other types of batteries for these applications. For example, the non-gassing characteristic of the Li-Al/FeS_x cell permits the battery to be built in a hermetically sealed jacket. This design feature gives the lithium/metal sulfide battery an important advantage over batteries that produce potentially explosive gases and require auxiliary systems to minimize the possibility of an explosion. Non-gassing batteries are especially important for application in submarines and mining vehicles.

An update and refinement of an earlier manufacturing cost study[1] has been initiated. This cost update will examine the manufacturing cost of recently designed Li-Al/FeS and Li-Al/FeS_2 cells that have been fabricated using cost-effective techniques. Manufacturing costs will be estimated for battery production in a pilot plant and in an automated plant.

B. Battery Design

1. Stationary Energy Storage Batteries
(S. Zivi, T. Fornek,† A. A. Chilenskas)

Conceptual design studies‡ of a 5.6 MW-hr battery module for stationary energy storage have been conducted at ANL and the Atomics International Division of Rockwell International; the resulting two conceptual designs are currently being merged into one. Testing of this type of module in the Battery Energy Storage Test (BEST) Facility is expected to take place in 1983. A preliminary design of this module is scheduled for completion late in 1978.

---

*Private consultants.

†Engineering Division, ANL.

‡Funded by the Department of Energy (DOE) and Electrical Energy Systems (EES).

2. Electric-Vehicle Battery
(J. Graae, T. E. Fornek, A. A. Chilenskas)

A conceptual design of an insulating jacket for a 40 kW-hr vehicle battery (Mark IA) has been initiated. The shape of this jacket will be prismatic in order to conform to the shape of present electric-vehicle cells. This shape results in a minimum of wasted space.* Because the battery jacket utilizes a vacuum-foil insulation, careful consideration must be given to the design and fabrication of a lightweight housing that can withstand atmospheric pressure without buckling.

*Recent studies at ANL suggest that volumetric energy density may be just as important a criterion as gravimetric energy density for many vehicle applications.

III. INDUSTRIAL CELL AND BATTERY TESTING
(W. E. Miller, E. C. Gay)

Testing of industrially fabricated lithium-aluminum/metal sulfide cells and batteries assembled from these cells is continuing. The improvements in cell designs that are demonstrated by this testing will be incorporated into future industrial cells. Fabrication of equipment for testing these cells and batteries continues. This equipment includes a facility to test large-scale (up to 60 kW-hr) batteries and another facility for lifetime testing of up to 100 industrial cells.

A. Testing of Contractor Produced Cells

Two industrial firms under contract with ANL--Eagle-Picher Industries, Inc. and Gould Inc.--are fabricating Li-Al/FeS and Li-Al/FeS_2 cells. These cells are being tested either at ANL or in their own laboratories. A performance summary of the Eagle-Picher and Gould cells operated during this quarter is presented in Appendix A.

The Atomics International Division of Rockwell International is continuing to fabricate and test Li-Si/FeS_x cells under a subcontract with ANL.

1. Qualification Testing of Eagle-Picher Cells
(T. D. Kaun, P. F. Eshman, J. R. Sink*)

Eagle-Picher has fabricated most of the 55 cells in their current subcontract with ANL. The designs of these cells were basically the same as those of the baseline FeS and FeS_2 cells (ANL-76-98, pp. 14-15), but with carefully selected variations (ANL-77-75, pp. 17-18). These variations included electrode thickness, capacity loading, separator material, position of the positive terminal rod, diameter of the positive terminal rod, and design of the positive current collector. The modified cells are evaluated using a standardized procedure that permits a comparison of the performance characteristics of cells with different designs.

Table III-1 presents performance data for Eagle-Picher FeS cells, and Fig. III-1 shows the utilization in the positive electrodes of these cells as a function of discharge current density. The utilization of the baseline cell with thin electrodes (1A) was much higher than that of the baseline cell with thick electrodes (1B). The specific energies of both types of these baseline cells were lower than those of the other FeS cells; this result is partially due to the lower loading of active material (higher electrolyte volume) in the baseline cells.

The negative electrodes were essentially the same thickness (same electrolyte volume) in the Type I3A and I3B cells; however, a thinner positive electrode was used in Cell I3B. This difference in cell design resulted in a better utilization but a lower ratio of active material to total cell weight in the Type I3B cell. Consequently, the specific energy of the Type I3B cell was about equal to that of Type I3A. In the Type I3C cell, the negative electrode was essentially the same thickness as that of the Type I3A and I3B cells, but the capacity loading of the electrode was increased 13% by decreasing its

*Cooperative Program Student.

Table III-1. Performance Data on Eagle-Picher FeS Cells

Cell Type[a]	Electrode Thickness, mm		Electrolyte[c] Volume, %		Capacity Loading, A-hr		Specific Energy, W-hr/kg			Peak Specific Power, W/kg
	Pos.[b]	Neg.	Pos.	Neg.	Pos.[b]	Neg.	40 mA/cm^2	60 mA/cm^2	80 mA/cm^2	
1A	3.25	3.5	67.3	30.7	70	70	47	43	--	42
1B	6.2	7.3	66.9	29.8	150	150	49	26	13	30
I1A[d]	5.9	6.7	67.0	20.0	150	170	54	30	15	30
I1B[d]	5.9	5.9	65.7	22.9	150	160	61	44	29	27
I3A	6.0	6.7	67.4	20.7	150	170	52	36	29	33
I3B	5.0	6.45	65.5	17.8	127	170	54	41	28	32
I3C	4.4	6.6	55.4	8.3	145	193	68	52	37	36

[a] At least two cells of each type were operated.

[b] Because the cells have two negative electrodes and one positive electrode, the positive electrode is considered to consist of two halves, each having the thickness given here. This dimension is referred to as "the half thickness."

[c] At full charge.

[d] Yttria felt substituted for the usual BN cloth as the electrode separator; these cells short-circuited in less than 84 days.

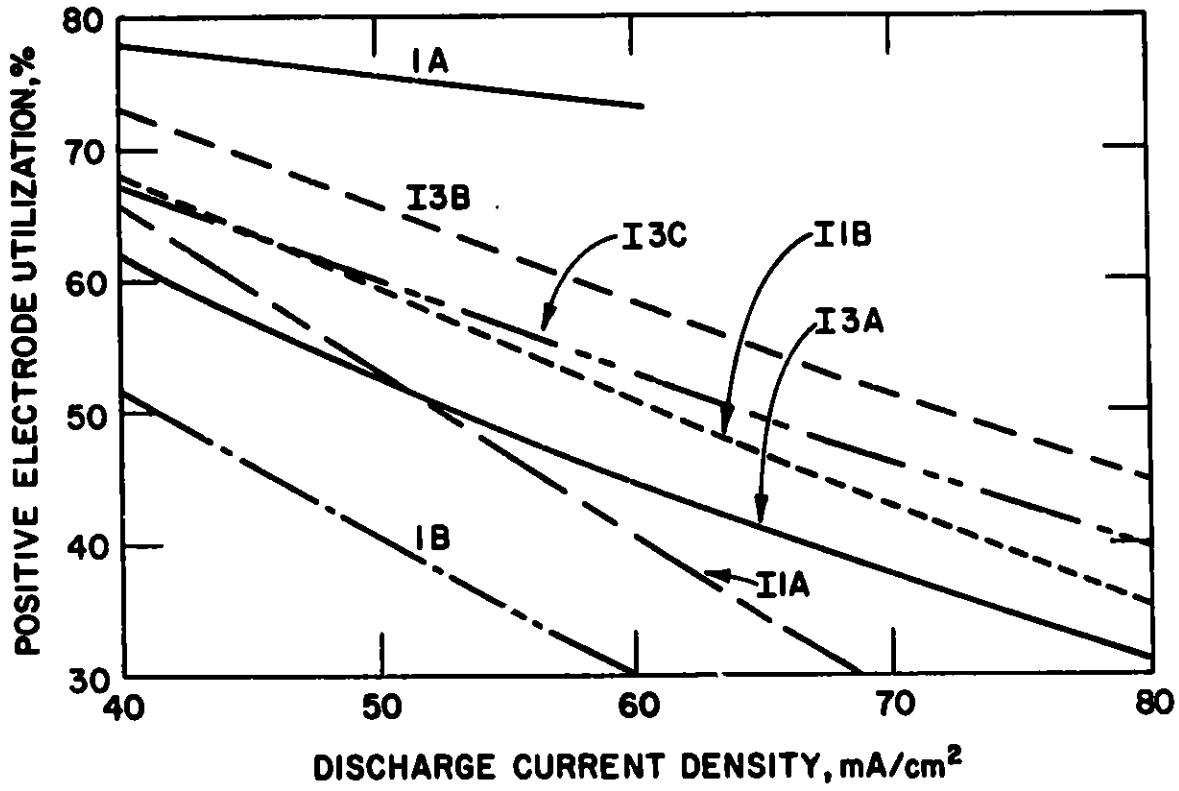

Fig. III-1. Utilization of Active Material in Eagle-Picher Charged FeS Cells

electrolyte volume. The positive electrode in the Type I3C cell was also more compact than that of the Type I3A and I3B cells; it had the same capacity loading as the positive electrode in I3A but was 73% as thick. The effect of the decreased electrolyte volume is clearly evident in that the utilization in I3C was lower than would have been expected on the basis of the decreased electrode thickness. However, the specific energy of I3C was higher than those of the Type I3A or I3B cells because of its high ratio of active material to total cell weight.

Table III-2 presents performance data for Eagle-Picher FeS_2 cells. and Fig. III-2 depicts the utilization of the positive electrode in these cells. The utilization is considerably higher for the Type 2A cell (thin electrodes) than for the Type 2B cell (thick electrodes); however, the specific energy of the Type 2B cell is higher because the ratio of active material to total cell weight is high enough to compensate for the loss in utilization. The Type I4 cells were tested to determine the effect of moving the positive terminal rod from the center line of the Type 2B cell to a position near one edge of the electrode; this change in cell design decreased both the utilization and specific energy. The Type I6 cell had a thinner and denser positive electrode (half-thickness, about 4.0 *vs.* 6.0 mm for the same capacity loading) and a denser negative electrode (about 30% more active material for the same electrode thickness) than the Type B cell. These modifications in the design of the Type 2B cell resulted in a decrease in

Table III-2. Performance Data on Eagle-Picher FeS_2 Cells

Cell Type[a]	Electrode Thickness, mm		Electrolyte[c] Volume, %		Capacity Loading, A-hr		Specific Energy, W-hr/kg			Peak Specific Power, W/kg
	Pos.[b]	Neg.	Pos.[b]	Neg.	Pos.	Neg.	40 mA/cm^2	60 mA/cm^2	80 mA/cm^2	
2A	3.3	3.3	78.0	21.3	70	70	64	56	46	67
2B	6.3	6.8	76.6	25.9	150	150	78	74	66	50
I4	5.9	6.4	76.6	15.8	156	170	61	55	48	40
I6	3.9	6.5	64.5	16.5	156	199	83	76	67	57
I7	5.2	6.6	62.1	8.9	222	230	91	86	80	65

[a]At least two cells of each type were operated.

[b]Because the cells have two negative electrodes and one positive electrode, the positive electrode is considered to consist of two halves, each having the thickness given here. This dimension is referred to as the "half-thickness."

[c]At full charge.

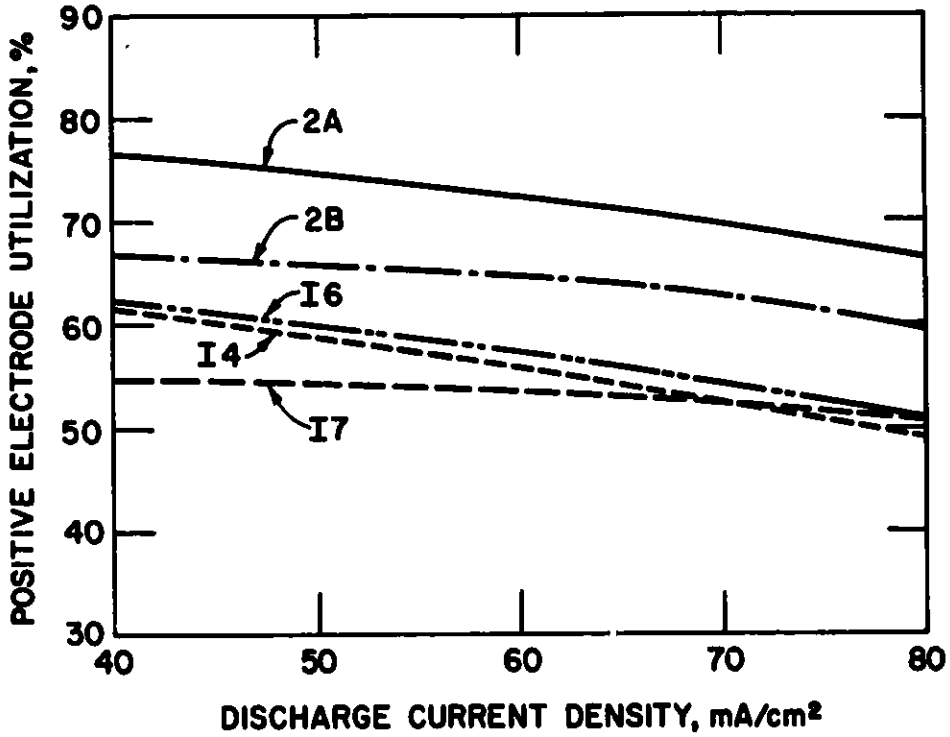

Fig. III-2. Utilization of Active Material in Eagle-Picher Charged FeS_2 Cells

utilization and a slight increase in specific energy. The Type I7 cell had a slightly thinner (half-thickness, ~5.0 mm) and denser (45% more active material) positive electrode than the Type B electrode; the negative electrode was denser (about 50% more active material for the same thickness); and the current collector had an improved design. These modifications in cell design resulted in the lowest utilization but the highest specific energy of any Eagle-Picher cell.

In general, utilization decreases as electrode thickness increases (constant electrolyte volume). The specific energy is higher in thicker-electrode FeS_2 cells than in thinner-electrode FeS_2 cells because the ratio of active material to total cell weight is high enough to compensate for the loss of utilization. In thicker-electrode FeS cells, the ratio of active material to total cell weight is usually not great enough (especially at high current densities) to compensate for the lower utilization. Thus the use of thin electrodes is probably more important in FeS than in FeS_2 cells.

A comparison of the data in Figs. III-1 and III-2 indicates the following. As the discharge current density increases, the utilization decreases much more rapidly in FeS cells (with the exception of the Type 1A cells) than in FeS_2 cells. The utilization curve for the Type 1A cells was similar to that of the Type 2A cells.

Six Eagle-Picher Type 2B cells in which BN felt was substituted for BN fabric (Cells I-8-A-1 to I-8-A-4 and I-8-C-9 and I-8-C-10) have been tested. All six cells short-circuited or exhibited poor coulombic efficiency within the first 20 cycles of operation. The primary cause of short-circuiting may be the poor quality of the BN felt used in these cells. The BN felt currently available is much stronger and easier to handle. Some modifications in cell design may be necessary to achieve acceptable lifetimes with cells using BN felt. Problems with sufficiently wetting the BN felt occurred in at least one cell (I-8-A-1), which had a peak specific power of 28 W/kg and a specific energy of 60 W-hr/kg at the 4-hr rate (current density, 84 mA/cm^2). A cell (I-8-A-4) with the same design but lower resistance had a peak specific power of 58 W/kg and a specific energy of 70 W-hr/kg at the 4-hr rate. Cells I-8-C-9 and I-8-C-10 contained 100-mesh molybdenum screens instead of the ZrO_2 cloth retainers used in the Type 2B cells; no change in cell performance was noted. Testing of these cells has indicated that a cell with a BN felt separator (sufficiently wet) has a lower resistance than one with a BN fabric separator--9 *vs.* 11 mΩ. This represents about a 13% improvement in power.

2. Testing of Eagle-Picher Cells
(V. M. Kolba, J. L. Hamilton, G. W. Redding, W. W. Lark)

Tests were conducted on Eagle-Picher cells to evaluate the effect on performance of various charging currents, elevated operating temperatures, and different negative-to-positive capacity ratios.

a. Charging Studies

An FeS cell, I-3-B-1 (see Appendix A and Table III-1 for a more detailed description of this cell), is being tested to determine the effect of different charge and discharge currents on performance. This cell has been cycled at discharge-charge currents* of 10, 15, 20, and 25 A as well as at a charge current of 10 A and discharge currents of 15, 20, and 25 A. After an initial slight loss, the capacity of the cell at charge-discharge currents of 10, 15, 20, 25 A (see Table III-3) has been very stable. During the last 34 cycles of operation, the coulombic efficiency has begun to decline. Use of a 10-A charge and a 15-A discharge current instead of a 15-A discharge-charge current resulted in a slight increase in capacity (2.5%) and energy (3.2%). The same effect on capacity and energy was seen when a 10-A charge and a 20-A discharge were used instead of a 20-A charge-discharge current. Use of a 10-A charge and a 25-A discharge current instead of a 25-A discharge-charge current resulted in an increase in capacity and energy of 4.8% and 7%, respectively.

b. Elevated Temperature Operation

The effect on performance of operating three Li-Al/FeS cells--1B4, I-3-B-1, and I-3-C-2 (see Table III-1 and Appendix A for a detailed description of these three cells)--at elevated temperatures (up to 500°C) has been investigated.

---

*The Eagle-Picher cells have an electrode surface area of 312 cm^2.

Table III-3. Performance Data on Cell I-3-B-1

Discharge-Charge Current, A	Cycle No.	Capacity, A-hr	Energy, W-hr
10	17	101.7	130.6
	46	95.0	121.3
	74	90.3	117.1
	175	88.6	116.4
	289	90.6	110.1
	385	90.6	109.9
	487	93.5	113.2
	562	83.9	99.8
15	8	88.4	107.5
	155	79	97.1
	253	82.2	109.4
	337	85.6	98.9
	441	85.3	98.7
20	82	77.3	92.4
	274	75.9	84.6
	362	76.7	85.4
	462	77.7	86.1
25	280	67.9	72.6
	375	66.9	71.4
	471	63.7	67.7

The operating temperature of Cells I-3-B-2 and 1B4 was raised from 425 to 500°C. The effects on performance of this temperature change are shown in Table III-4. (These data are average values over five cycles at each current setting.) These preliminary results indicate that the cell performance increases when the operating temperature is raised from 425 to 500°C; however, the long-term effects of operating a cell at 500°C remain to be evaluated. In general, the improvement in capacity was greatest for Cell 1B4 (~49% at 10 A and 82% at 15 A).

The operating temperature of these two cells was reduced to 425°C. The effects on performance of this change are shown in Table III-5. With the return of the operating temperature to 425°C, the capacity of Cell I-3-B-2 declined 7.7% and that of Cell 1B4 declined 26.4%. In Cell 1B4 an additional capacity decline of 11% occurred over the nine cycles following the temperature reduction. However, the capacity of Cell 1B4 has shown an overall increase of 22.6% since the beginning of these thermal tests. Cell I-3-B-2 showed only an additional 2% decline in capacity over the nine cycles subsequent to the temperature reduction.

Cell I-3-C-2 was chosen for thermal testing because the capacity and energy during 375 cycles of operation declined more than 35%, but the coulombic and energy efficiencies remained high. Thus this cell did not have an internal short circuit, and the reason for the declining performance could not be explained.

Table III-4. Performance Data on Cells 1B4 and I-3-B-2 after Operating Temperature Raised from 425 to 500°C

	Cell 1B4		Cell I-3-B-2	
	425°C	500°C	425°C	500°C
Capacity, A-hr				
at 10-A current	61.1	90.8	94.5	104.9
at 15-A current	39.7	72.3	---	91.5
Energy, W-hr				
at 10-A current	71.4	105.8	115.8	126.9
at 15-A current	44.1	82.1	---	106.3
Average Voltage, V				
at 10-A current	1.169	1.165	1.225	1.210
at 15-A current	1.111	1.136	---	1.162

Table III-5. Performance Data on Cells 1B4 and I-3-B-2 after Operating Temperatures Reduced from 500 to 425°C

	Cell 1B4		Cell I-3-B-2	
Data[a]	500°C[b]	425°C[c]	500°C[b]	425°C[c]
Capacity, A-hr	74.6	54.9	81.8	75.5
Energy, W-hr	83.7	60.3	94.0	86.9
Average Voltage, V	1.122	1.098	1.149	1.151

[a]All measurements made at a current of 15 A.

[b]Measured immediately preceding temperature reduction.

[c]Measured two cycles after temperature reduction.

The operating temperature of this cell was adjusted to 410, 425, 450, 475, 500, and 525°C. The performance of the cell at these various temperatures (charge-discharge current, 10 A) is shown in Fig. III-3 (the voltages given in this figure are average values). As can be seen in this figure, at temperatures above 450°C, the cell capacity improved markedly; however, very little additional improvement in capacity occurred at temperatures above 475°C. The specific energy of the cell on cycle 422 was 68 W-hr/kg at the 10-hr rate; this is about a 7% increase in specific energy from that early in cell life (cycle 4). The temperature of this cell will be returned to 425°C in increments of 25°C.

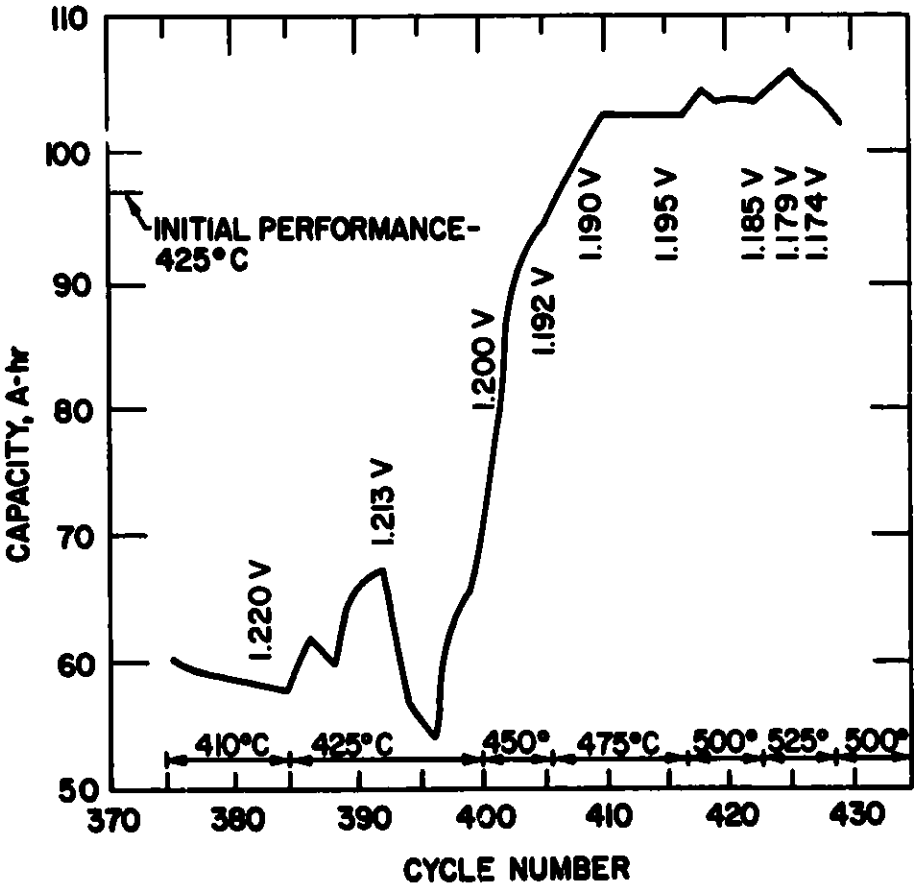

Fig. III-3. Effect of Temperature on Operation of Cell I-3-C-2

The reasons for the above thermal effects have not been determined. However, several possibilities have been proposed: off-eutectic electrolyte, solubility changes in J phase ($LiK_6Fe_{24}S_{26}Cl$), rate changes, or changes in electrode morphology. Further testing will be conducted to determine the mechanisms for these thermally induced effects.

c. Variations in Negative-to-Positive Capacity Ratio

Tests were conducted to evaluate the effect on performance of different negative-to-positive capacity ratios in FeS_2 cells. Cell I-8-F-17 has a thin (Type A) positive electrode and thick (Type B) negative electrodes; the capacity loading is 170 A-hr for the negative electrode and 71 A-hr for the positive electrode. Cell I-8-G-19 has a thick (Type B) positive electrode and thin (Type A) negative electrodes; the capacity loading is 80 A-hr for the negative electrode and 157 A-hr for the positive electrode. Cell I-8-F-17 is a two-plateau cell and Cell I-8-G-19 is an upper-plateau cell.* Both cells were charged and discharged at a current of 10 A. Performance data for these two cells are presented in Table III-6.

Table III-6. Performance Data on Cells I-8-F-17 and I-8-G-19 As a Function of Cycle Number

	Cycle No.							
	5	10	15	20	25	30	40	45
Capacity, A-hr								
I-8-F-17	57.1	55.4	--	53.3	52.2	50.6	50.9	50.3
I-8-G-19	62.2	61.9	58.9	56.8	53	55.8	54.8	51.2
Utilization,[a] %								
I-8-F-17	80.4	78	--	75	73.5	71.3	71.7	72.1
I-8-G-19	77.8	77.4	73.6	71	66	69.8	68.5	64
Energy, W-hr								
I-8-F-17	78.7	76.3	--	73.2	71.6	69.1	69.1	68.3
I-8-G-19	95.2	94.7	89.6	85.9	80.0	86.5	84.1	78
Ave. Voltage, V								
I-8-F-17	1.378	1.377	--	1.373	1.372	1.366	1.358	1.350
I-8-G-19	1.531	1.530	1.521	1.512	1.509	1.550	1.534	1.523

[a]Utilization of the electrode that limited cell capacity

Both cells had high resistances, ∿13.2-14.8 mΩ; the reason for this is unclear at present. Operation of Cell I-8-G-19 was terminated after 85 cycles because of declining coulombic efficiency; this was probably caused by a malfunction of the cell temperature controller on cycle 30. The capacity decline by the 45th cycle was about 12% for I-8-F-17 and about 18% for I-8-G-19. The voltage decline was about 28 mV for the former cell and 8 mV for the latter cell. These preliminary results indicate slightly better performance for Cell I-8-F-17 than for I-8-G-19.

*These cells are operated only on the upper of two voltage plateaus that are characteristic of FeS_2 cells.

3. Testing of Gould Cells
(T. D. Kaun, P. F. Eshman, J. R. Sink)

Gould Inc. has fabricated 32 upper-plateau FeS_2 cells of the 55 cells in their current subcontract with ANL. The Gould cells consist of hot-pressed (13 x 18 cm) electrodes that are assembled in the uncharged state. These cells are being tested to determine the effect on performance of (1) current collector design, (2) lithium content in the negative electrode, (3) electrolyte volume and thickness of the positive electrode, and (4) method of particle retention.

The following mode for testing Gould cells was established by both ANL and Gould: discharge current densities of 33, 66, and 100 mA/cm^2 with a discharge cutoff voltage (IR-free) of 1.3 V, and a current-limited (33 mA/cm^2), constant-voltage (2.2 V) charge. This cycling mode is expected to provide data for determining the optimum electrode design of this type of cell. A seven-day cycling schedule (computer controlled) was selected for these tests. Graphs of voltage *vs.* capacity, specific energy *vs.* discharge rate, and specific power *vs.* discharge rate will be made for each cell.

Preliminary testing was conducted on three Gould cells with 45.2 at. % lithium in the negative electrode, namely, G-04-013, G-04-013A, and G-04-025. The utilization of these electrodes (theoretical capacities, 180 A-hr) was expected to be 65% at a current density of 33 mA/cm^2, but only 40-45% utilization was obtained. A fourth Gould cell, G-04-009A, which had 50.0 at. % lithium in the negative electrode, was also tested. This electrode had satisfactory utilization, 60% at 33 mA/cm^2.

At discharge current densities ranging from 33 to 133 mA/cm^2, the capacity of Cell G-04-013 varied by only 15%. Cell G-04-013A also showed the same small variance in capacity over this discharge range. The peak capacity for these two cells was 122 A-hr. Cell G-04-013 was operated for 68 cycles with a 6.8% decline in cell performance. Figures III-4 and III-5 present the specific energy and peak specific power for G-04-013A. The range of resistances for the Gould cells was 6 to 9 mΩ.

4. Cell Testing at Atomics International

A number of positive electrode structures were fabricated in the uncharged condition with internal constraint against swelling forces, and tested in electric-vehicle bicells. Dual-faced electrodes using multiple vertical ribs have been selected for intensive investigation. These electrodes will be evaluated on the basis of performance, ease of fabrication, and potential cost as compared with the honeycomb electrodes used earlier. The porous nickel or nickel screen particle retainers can be diffusion-bonded to the nickel ribs before the structure is loaded with the active material, thereby reducing the hazard of bond failure caused by bond-zone contamination.

An electrode of this type, using nickel screen rather than porous nickel retaining members for the active material, has shown low internal resistance and superior performance at high rates (90 mA/cm^2). This is attributed to the lower tortuosity of the screen.

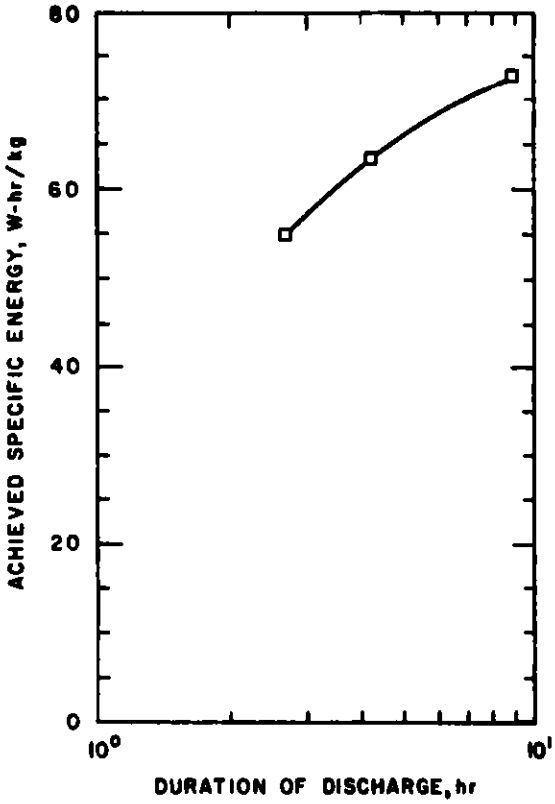

Fig. III-4.

Specific Energy of Cell G-04-013A

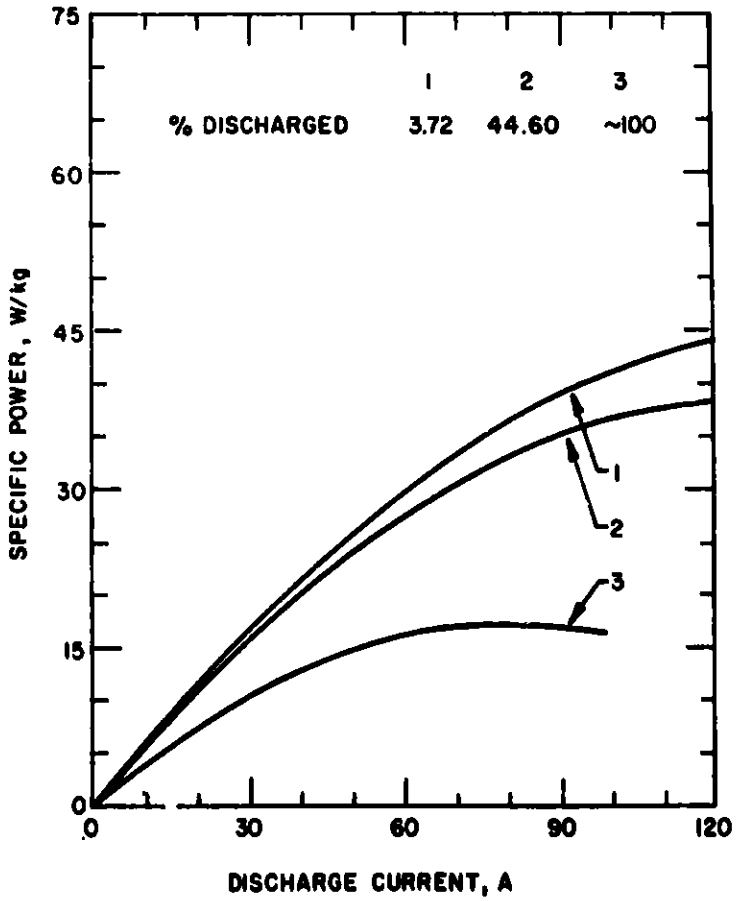

Fig. III-5.

Peak Specific Power of Cell G-04-013A at 3.7%, 44.6%, and 100% Discharge

Fabrication of a Li-Si/FeS cell (2.5 kW-hr) has been completed. This cell will be placed in operation next quarter.

A summary report of the research activities for FY 1977 has been prepared.

B. Battery Testing

(V. M. Kolba, G. W. Redding, J. L. Hamilton)

The battery testing efforts are directed toward the development and evaluation of battery configurations and designs. The performance of cells in series and parallel arrangements is being evaluated, and start-up and conditioning methods are being investigated. A summary of battery performance data is given in Appendix B.

In November, proposals were solicited for the development, design, and fabrication of a 40 kW-hr battery, designated Mark IA, to be tested in an electric van at ANL early in 1979. The statement of work calls for a 40 kW-hr battery package consisting of two 20 kW-hr modules, which will be fabricated and delivered to ANL in 12 months. The energy storage capability is to be greater than 40 kW-hr at the 4-hr rate after 60 equivalent deep discharges, and the power is specified as 30 kW for a 15-second pulse at a 50% state of charge. The maximum weight of the Mark IA battery is 680 kg and the maximum volume is 400 L. The operating temperature will be between 400 and 500°C, with a maximum heat loss of 400 W. The battery cells are expected to be of a multiplate design employing Li-Al or Li-Si negative electrodes and FeS positive electrodes with molten LiCl-KCl electrolyte.

1. Two-Cell Battery Test

Operation of Eagle-Picher FeS Cells 1B4 and 1B6 in series (designated Battery B7-S) has been terminated after 491 days and 803 cycles. The reasons for termination of the operation of this battery were poor capacity and coulombic efficiency. Cell 1B6 had short-circuited; cycling of Cell 1B4 is continuing (see Section III A.2.b.).

2. Three-Cell Battery Test

After 75 cycles the three Eagle-Picher FeS_2 cells (I-5-4, I-5-5, and I-5-7) comprising Battery B12-S (ANL-77-75, p. 21) were connected in parallel and operated in an insulated housing. This battery (designated B13-P) showed a peak capacity of 290 A-hr and a peak energy of 398 W-hr at a 30-A discharge current. This corresponds to specific energy for the cells of 62 W-hr/kg. After 17 cycles, coulombic efficiency was very low. Attempts to improve the performance over the next 21 cycles were not successful; therefore, testing was terminated. Post-test examination of Cells I-5-4 and I-5-7 showed that they had short-circuited. Attempts were made to continue to operate Cell I-5-5; however, it had poor coulombic efficiency and the test was terminated.

C. Equipment for Cell and Battery Tests

A facility for testing up to 100 industrial cells is presently being constructed at ANL; to be included as an integral part of this facility is a computer system for monitoring of cell performance and data acquisition. This facility will be used primarily for lifetime testing of industrial cells. A facility is also being constructed for laboratory tests of large-scale (up to 60 kW-hr) electric-vehicle batteries that will precede in-vehicle tests. This facility will have the capability for computer-controlled cell operation and data-acquisition. In addition, equipment for in-vehicle testing of batteries is being designed.

1. Testing Facilities for Cells and Batteries

a. Test Facility for 12 Cells
(G. W. Redding, J. L. Hamilton, R. Alford,* V. M. Kolba)

Fabrication of a facility for testing up to 12 cells has been completed and it is now operational.

b. Test Facility for 100 Cells
(J. D. Arntzen, V. M. Kolba, W. E. Miller)

Plans are being made to build a 100-cell test facility, which will be used to determine product and performance reliability prior to procurement of large numbers of electric-vehicle cells. The emphasis will be on lifetime testing of large numbers of cells supplied by industrial contractors. This form of testing is required to provide meaningful performance and lifetime statistics on the industrially-fabricated cells.

An area at ANL is being renovated to accommodate 50 stations for cell testing. Later, another 50 stations will be added. A plan for an air-conditioned enclosure to house the data-acquisition system for the facility has been submitted. The ANL Electronics Division is currently building a prototype cycler for the individual stations (see Section III.C.3). The power supply for the cycler has been received. Following testing and debugging of this cycler, bids will be solicited for the purchase of 50 cyclers from outside contractors.

The individual cell testing stations will include a steel drum filled with rigid insulation containing heating elements. The cell will be suspended from the lid of the drum along with heat shields and insulating material. Each drum will be positioned on an open relay rack which will support the cycler, power supply, and furnace control panel. The drums will be maintained under a positive-pressure argon blanket to reduce atmospheric corrosion.

Most materials for the individual stations have been received. Components that are on order include temperature controllers, electrical feedthroughs, relay racks, and argon pressure regulators.

---

*Industrial participant from Eagle-Picher Industries, Inc.

Electrical power requirements for the facility have been reviewed, and available power has been determined to be adequate. An existing argon manifold on the service floor beneath the facility will be tapped to provide an inert gas blanket for the test units.

c. Stationary Testing Facilities for Batteries
(V. M. Kolba, W. E. Miller)

Equipment, instrumentation, and support items for static testing of large scale (30-60 kW-hr) batteries have been specified, and are being procured. These items will be installed, and checked out before midyear 1978. The data acquisition and control systems have been ordered. Drawings were completed for the equalizer system, and power supplies have been procured for this system. A submodule of the equalizer is being fabricated.

d. Equipment for Testing Batteries in Vehicles*
(A. A. Chilenskas, E. R. Hayes, S. A. Box, W. W. DeLuca, F. Hornstra)

A Renault automobile has been obtained. At present, this vehicle is powered by a 72-V lead-acid battery. Substitution of one 6-V lithium/metal sulfide battery module for a 6-V lead-acid battery module is planned for the first in-vehicle test of the advanced battery. Testing of this type of a battery in a vehicle will provide input data for the Mark IA design. In addition to the Renault, a van powered by lead-acid batteries will be used to assist ANL personnel in developing instruments for in-vehicle testing of lithium/metal sulfide batteries.

In this period, the following tasks for in-vehicle testing were addressed: (1) on-board instrumentation for battery performance evaluation and (2) design of a battery charger.

For the first of these two tasks, an instrumentation package is being designed for in-vehicle measurements of battery parameters related to vehicle operation. Preliminary equipment specifications have been outlined. Digital data recording was selected over an analog scheme due to the volume of data and stability of the overall system that is required to obtain accurate data. Analog signals from the battery and vehicle will be converted to digital values and stored on magnetic tape in a format suitable for direct playback into a computer for analysis. Temporary storage is provided for data manipulation (data formatting or scaling or any general processing for recording) before storage. Local digital displays are available for ease of calibration and testing of the instrumentation system before in-vehicle testing as well as for maintaining vehicle and battery operating characteristics. The central controller is a microprocessor which executes command functions as pre-programmed in the local program read-only-memory (PROM). An interrupt unit is available which can be utilized to command the microprocessor to respond to particular events or "road-load conditions."†

---

*Funded by the Department of Energy (DOE), Division of Transportation Energy Conservation (TEC).

†This refers to operating conditions (such as road grades, acceleration, and braking) which affect the power output of the battery.

The package will have a modular construction for ease of maintenance and flexibility. Replacement of the program element or card is the only action required to alter system operation. The "on-board" system can be configured in a simplified form with relatively few analog input points (16). Direct data storage will be used for the initial road tests. This system can easily be expanded to 64 analog input points with data acquisition that is a function of road-load conditions. At present, the possibility of using commercially available components that can be packaged and programmed for this application is being investigated.

A charging system suitable for mass-produced electric-vehicle batteries must be economical, lightweight, reliable, and simple to use. Such a charging system requires two separate chargers: a high-current main charger and a charge equalizer. Both of these chargers must have the capability to operate from standard power sources on a daily basis. A contract has been issued to TRW Systems to perform a design and cost study for an electric-vehicle battery (Li-Al/FeS_x) charger. Both "on" and "off" board systems will be investigated. The "on-board" system has a weight restriction, but can share components from the vehicle's traction control system.

The first contract meeting between TRW representatives and ANL personnel was held at ANL on 14 December 1977. From the information obtained, TRW can now assess the charger requirements for an electric vehicle. They will soon generate a detailed set of charger specifications.

In conjunction with this program, a computer analysis was performed on two chargers using different regulation techniques. Neither charger contained a transformer. The first utilized resistive current limiting, whereas the second utilized silicon-controlled-rectifier (SCR) current regulation. The analysis showed that the solid-state charger has the potential for higher charging efficiencies, but a filter must be used to achieve the high charging efficiency. At currents of 10 to 25 A, a filter is practical in terms of size and cost. Optimization of the relative amplitudes of the input ac power and battery voltages also improves efficiency, but at a sacrifice to the maximum charging rate. This matching can be easily accomplished by utilizing a transformer. Use of a filter, however, improves efficiency without decreasing the maximum charging rate.

Data obtained from subsequent operation of a solid-state charger (without a filter) on a Renault electric vehicle* were in close agreement with the computer analysis data. The charger is presently being modified to incorporate a filter circuit.

*This vehicle used lead-acid batteries.

2. Data-Acquisition and Control Systems for Battery and Cell Testing
(C. A. Swoboda, F. Hornstra)

Studies of the data-acquisition and control systems for advanced batteries resulted in recommendations detailing two independent systems. The first is to be used for a 40 kW-hr battery test. Integration of the computer with a CAMAC* system has undergone testing at Kinetic Systems in Lockport, Illinois. The second system is a multi-user facility. This system will initially support three cell and battery testing laboratories and the 100-cell testing facilities. Bid review and source selection of the system components are now under way.

3. Electronics Development
(W. W. Lark, F. Hornstra)

A second-generation minicycler (MARK II) will be fabricated by Paraplegics Inc. Thirty units have been ordered and will be available for cell testing by January 1978. The MARK II minicycler is identical to the MARK I minicycler with the following two exceptions: set-up of the units and direct interface to our "watchdogs."†

The 100-A battery and cell cyclers being fabricated by the ANL Electronics Division will be delivered during January 1978. A total of six units plus the prototype will then be available for cell/battery testing under either manual or computer control. A design has been approved for a 75-A cycler for the cell testing facility. The prototype will be fabricated by the ANL Electronics Division. This unit will be similar to the 100-A cycler but will not have the capability for computer control or constant-power discharge.

---

*The CAMAC system is an international, modular data-acquisition and control standard which, when interfaced to a computer, allows the use of remote stations to gather data and control various types of equipment used in industrial as well as specialized research projects.

†If the battery voltage exceeds a preset upper limit or declines below a preset lower limit as set on the "watchdog," the battery is placed on an open circuit.

IV. CELL DEVELOPMENT AND ENGINEERING
(H. Shimotake, E. C. Gay)

The effort in this part of the program is directed primarily toward the development of engineering-scale, prismatic cells capable of meeting the requirements for electric-vehicle batteries. Recent cell development work has concentrated on improving lifetime and specific energy at high discharge current densities (>100 mA/cm^2), and on establishing improved fabrication techniques. Whenever advances in cell technology are demonstrated at ANL, these advances are incorporated as quickly as possible into the industrial cells.

During this quarter, investigations were carried out on: (1) the use of nickel sulfide in the positive electrode as a total or partial substitute for FeS_2, (2) the use of highly conductive carbon additives in FeS cells, (3) the use of metal additives in Li-Al electrodes, and (4) the use of powder separators in FeS cells. A summary of cell performance data is presented in Appendix A.

A. Cells with Nickel Sulfide in the Positive Electrode

Cell chemistry studies (ANL-77-75, pp. 52-53) have indicated that NiS_2 may be an attractive alternative to FeS_2 as the active material in the positive electrode. Consequently, the recommendation was made that the use of NiS_2 as a substitute for the active material in the positive electrode or as an additive in Li-Al/MS_2 cells be investigated in engineering-scale cells.

1. Semicharged Cells with Pressed Electrodes
(L. G. Bartholme)

Engineering cells containing different amounts of nickel sulfide in the positive electrode were tested. These cells had theoretical capacities of 110-120 A-hr and BN fabric separators. The positive electrodes were hot-pressed, and assembled in a semicharged condition. Table IV-1 presents the active material composition (at full charge) and the specific energy and lifetime of these cells; an FeS_2 cell (R-26) is also presented for comparison purposes. As can be seen from this table, the nickel sulfide cells have lower specific energies than the FeS_2 cells; however, two of the nickel sulfide cells have operated for relatively long periods with little decline in capacity. Efforts are under way to determine a positive-electrode composition that will provide optimum cell performance and lifetime. The cost of nickel must also be taken into consideration in determining this optimum composition.

2. Charged Cells with Pressed Electrodes
(F. J. Martino)

Charged FeS_2 cells, designated "M-series" cells, were designed as compactly as state-of-the art technology would permit. In addition, BN or Y_2O_3 felt separator/retainers were used in these cells. The design of this type of cell is shown in Fig. IV-1.

Three M-series cells were reported in ANL-77-35, p. 31 and ANL-77-68, p. 28. A modification in the design of the cell housing of M-2 and M-3 resulted in a 10% decrease in weight from that of M-1. The specific energies

Table IV-1. Performance of Engineering Cells with Nickel Sulfide Electrodes

Cell No.	Positive Electrode: Composition of Active Material[a]	Positive Electrode: Carbon Powder Additive, wt %	Sp. Energy[b] W-hr/kg	Cycle Life
R-30	$FeS_{1.65}$ (78.8) $CoS_{1.65}$ (8.2) $NiS_{1.65}$ (13.0)	10.0	50	70
R-31	$NiS_{1.9}$ (90.7) CoS_2 (9.3)	0	40	>230
R-32	NiS_2 (100.0)	5.5	40	>160
R-33	NiS_2 (50.0) FeS_2 (50.0)	8.0	38	90
R-26	FeS_2 (96) CoS_2 (4)	0	70	240

[a]Composition at full charge; numbers in parentheses indicate mol % of each constituent.

[b]At a current density of 100 mA/cm^2 (about the 4.5-hr rate).

of these three cells were very high, but the cell lifetimes were very short. In order to produce stable performance and longer lifetimes, the next cell in this series, M-4, was built with a combination of iron sulfide and nickel sulfide (69 mol % $FeS_{1.46}$-31 mol % $NiS_{1.46}$) in the positive electrode; molybdenum powder (5.3 wt %) was added to improve conductivity. Yttria felt was used as the separator material. (This cell was described previously in ANL-77-75, p. 25.) The individual weights of components in three M-series cells are presented in Table IV-2, and performance data for these cells are presented in Table IV-3. Cell M-4 has achieved a specific energy of 85 and 70 W-hr/kg at the 4- and 2-hr rates, respectively. The specific peak power (taken with 15-sec power pulses) is about 143 W/kg at 100% charge, 88 W/kg at 50% charge, and 60 W/kg at 25% charge. After 170 cycles and 83 days of operation, the capacity of cell M-4 has declined less than 10%; present cell capacity is about 97 A-hr. Coulombic efficiency remains at 97%, and cell resistance is stable at about 3.3 mΩ. This cell has shown the best performance of any cell built with nickel sulfide in the positive electrode.

3. Cells with Carbon-Bonded Electrodes
(T. D. Kaun)

A carbon-bonded* cell (KK-13) using nickel sulfide in the positive electrode was recently fabricated. A mixture of Li_2S and Ni_7S_6 was sintered at 800°C in a helium atmosphere, and then ground to -100 mesh. The positive electrode was fabricated in a semicharged state from 88 mol % NiS_2-12 mol % CoS_2. The design of Cell KK-13 was similar to that of the

*See ANL-77-18 for a description of the carbon-bonding technique.

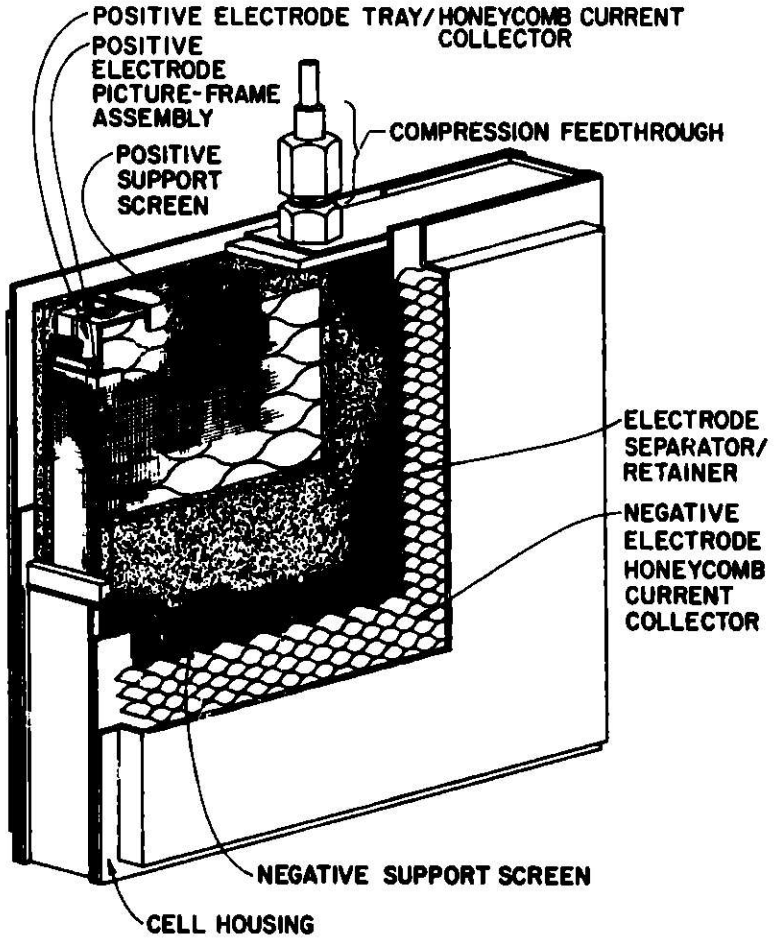

Fig. IV-1. Design of M-Series Cell

Table IV-2. Component Weights of Three M-Series Cells

	Weight, g		
	Cell M-1	Cell M-2	Cell M-4
Positive Active Material	329	327	377
Negative Active Material	218	219	209
Positive Current Collector	210	206	194
Negative Current Collector	192	244[a]	267[b]
Separator/Retainer	86	55	85
Electrolyte	583	536	464
Cell Can	381	57	47
Feedthrough	157	157	157
Total	2160	1801	1800

[a] Includes 132 g also serving as cell can.

[b] Includes 162 g also serving as cell can.

Table IV-3. Performance Data on Three M-Series Cells

Cell No.	Ave. Voltage, V	Max. Capacity,[a] A-hr	Specific Energy,[a] W-hr/kg	Energy Density[a] W-hr/L	Lifetime, Cycles
M-1	1.45	143	100	292	17
M-2	1.47	141	115	364	31
M-4	1.43	111	89	281	>170[b]

[a]At the 5-hr rate.

[b]Cell still operating.

M-series cell (Fig. IV-1) except that (1) the positive electrode was carbon-bonded instead of hot-pressed and (2) sheets of Y_2O_3 felt were placed at the electrode faces and BN fiber was packed around the electrode edges. In the latter case, the poor wettability of the BN permitted the elimination of excess electrolyte (about 50 g around the electrode edge).

Cell KK-13 has operated for more than 100 cycles (70 days) with 99.5% coulombic efficiency and less than a 6% decline in capacity. No erratic behavior in cell resistance or capacity has been exhibited. The cell has achieved specific energies of 81 and 100 W-hr/kg at the 4-hr and 8-hr rates, respectively.

The effect of operating temperature on the performance of Cell KK-13 was investigated. Cell resistance was found to change with respect to operating temperature as follows: ∿3.5 mΩ at 455 ± 10°C, ∿4.5 mΩ at 430 ± 10°C, and ∿5.5 mΩ at 415 ± 10°C. This resistance differential was constant throughout the discharge cycle.

B. Cells with FeS Positive Electrodes

In the past, two types of metal sulfides have been used as the active material in the positive electrode--FeS and FeS_2. The FeS_2 electrode is capable of high specific energy and specific power, but has the disadvantages at present of limited lifetime and the requirement for expensive current-collector materials. Consequently, the FeS electrode has been selected for the first electric-vehicle battery (Mark IA). Efforts are currently under way to develop an FeS cell that meets the performance goals for the Mark I battery.

1. Engineering-Scale Cell Tests
(L. G. Bartholme, F. J. Martino)

In ANL-77-75, p. 27, experiments on small-scale cells indicated that the addition of heat-treated carbon powder (1000°C) to the positive electrode of FeS cells would improve cell performance. Thus an engineering-scale cell (R-34) was constructed with 10 wt % carbon powder added to the FeS-Cu_2S electrode. The positive active material and the carbon powder were pressed into eight tile-like plaques, and then placed on both sides of a thin steel tray

(the current collector). The plaques were not pressed onto the tray. Good utilization was obtained--78% at the 4-hr rate (current density, 72 mA/cm^2). This cell continues to operate without capacity decline.

An "M-series" cell, M-5, was used to test NiS as an alternative to Cu_2S as an additive in FeS positive electrodes. This cell had a design that was similar to that of the other M-series cells (Fig. IV-1), except that the positive terminal rod and current collector tray were fabricated from nickel, and attached to a honeycomb structure made of molybdenum. This type of current collector allowed the use of higher charge cutoff voltages (typically set at 1.7 V). At the 4.5-hr discharge rate (current density, 52 mA/cm^2), this cell achieved a specific energy of 53 W-hr/kg; this is the best specific energy achieved by an FeS cell. The cell resistance is 3.3-5.7 mΩ, and the peak specific power is 120 W/kg at 100% charge, 65 W/kg at 45% charge, and 61 W/kg at 20% charge. After 80 cycles (83 days), the cell capacity declined 16%; this large drop in capacity is probably the result of a short circuit. Operation of this cell will soon be terminated, and the cell will be examined to determine the cause of failure.

2. Small-Scale Cell Tests
(K. E. Anderson, D. R. Vissers)

Experiments on small-scale cells are being undertaken to further define the optimum conditions for the preparation of FeS electrodes. The parameters which are being evaluated include the following: cell operating temperature, electrolyte composition, electrolyte volume in the positive electrode, and various additives (mainly carbon and metal sulfides) to the positive electrode. The cell design for these studies utilizes horizontally mounted electrodes with effective areas of ∿15.6 cm^2. The capacities for these cells are limited by the positive electrode (theoretical capacity: 6.5 A-hr in positive electrode and 10 A-hr in negative electrode). Boron nitride cloth wrapped around the positive electrode serves as the separator. The positive electrode housing is designed to minimize swelling. However, the porosity of the electrodes will be evaluated after cycling to ensure accurate measurements of cell performance characteristics.

Two such cells, one with FeS and the other with $Ni_{0.5}Fe_{0.5}S$ in the positive electrode, were assembled in the uncharged state. Heat-treated carbon powder was used as an additive. Both cells had substantial increases in utilization of the active materials when the temperature was increased from 450 to 500°C: the utilization* of the FeS cell increased from 41 to 64% and that of the $Ni_{0.5}Fe_{0.5}S$ cell increased from 59 to 78%.

A second FeS cell was used to evaluate the use of graphite fiber additive in the positive electrode. When the temperature of this cell was increased from 450 to 500°C, the utilization increased from 47 to 66%. The LiCl composition of the electrolyte in this cell was shifted from 58 to 67 mol % as the result of a suggestion by the Cell Chemistry Group.

*All utilizations in these studies were measured at a charge-discharge current density of 50 mA/cm^2.

The purpose of this shift was to lower the potassium ion concentration of the electrolyte, thereby reducing the amount of J phase ($LiK_6Fe_{24}S_{26}Cl$) formed in the positive electrode. Previous studies (ANL-77-17, p. 45) had indicated that the presence of J phase in an electrode tends to lower performance. This additional LiCl in the electrolyte increased the utilization from 47 to 85% at 450°C and from 66 to 92% at 500°C. A secondary result of this LiCl addition is that the thermal effect decreases. Prior to the addition of the LiCl, utilization increased by ∿40% when the temperature was raised from 450-500°C; after the LiCl addition, utilization increased by only 8% with this same increase in temperature.

C. Cells with Negative Electrode Additives
(F. J. Martino)

A series of tests were conducted to determine the effects of the addition of a third metal to the Li-Al electrode on FeS cell performance. Cells FM-0 (no additive), FM-1 (Li-Al-In), FM-2 (Li-Al-Ca), and FM-3 (Li-Al-Sn) were reported in ANL-77-68, p. 31. Cell FM-4, which had 5 wt % zinc added to the Li-Al electrode, operated for 207 cycles and 103 days. During the first 100 cycles, its performance was the same as that of the baseline cell (FM-0). During the second 100 cycles of operation, the capacity began to decline. When cell operation was terminated, the capacity had declined by ∿28%, to ∿37 A-hr (43% negative electrode utilization). The resistance was steady, ranging from 6.8 to 7.5 mΩ; the coulombic efficiency was 91%.

Owing to the good performance of the FeS cell with tin additive in the negative electrode, an FeS_2 cell utilizing Li-Al with a 6.6 wt % tin additive was placed in operation. This cell, designated FM2-1, showed nearly indentical performance to that of a baseline cell. Thus no improvement in performance was found in FeS_2 cells with tin added to the negative electrode.

D. Cells with Advanced Separators
(T. W. Olszanski)

Testing of powder separators in engineering cells is continuing (see ANL-77-75, p. 31). Two methods of incorporating powder separators into cells are also being evaluated: the vibratory-loading and hot-pressing techniques. The major advantages of powder separators are low cost and ease of fabrication.

Cell PW-8, an engineering-scale FeS cell, was built with a MgO powder separator (-60 to +120 mesh, 0.318-cm thick) that was filled in the cell by the vibratory technique. It contains screens and frames on both the positive and negative electrodes. This cell has operated for about 100 cycles and 75 days. The coulombic efficiencies during this time have been >98%; internal resistance has averaged 8-9 mΩ. Utilization of the FeS positive electrode at 450°C and a discharge-charge current density of 10 mA/cm^2 is ∿51%. At 520°C and the same current density a utilization of 73% was obtained. It is expected that the higher temperature inhibits formation of J phase, thereby yielding higher utilization of the positive active material.

A new candidate for a powder separator, CaS, is undergoing evaluation in a cylindrical (7.5-cm dia) FeS cell. The low density and potential low cost of this material makes this a very attractive separator candidate. This cell has operated for 51 cycles and 45 days. Coulombic and energy efficiencies are consistently >99% and >82%, respectively. Utilization of the cell at a discharge-charge current density of 55 mA/cm^2 is ∿50%.

E. Performance Assessment of Recent ANL Cells
(H. Shimotake)

Figure IV-2 plots the specific energy *vs.* the current density for three engineering cells that were operated during this quarter--R-34, M-4, and KK-13. Cell R-34 has a pellet positive electrode (FeS-Cu_2S), Cell M-4 has a pressed positive electrode ($FeS_{1.46}$-$NiS_{1.46}$), and Cell KK-13 has a carbon-bonded positive electrode (NiS_2-CoS_2). The shaded area represents the specific energy goal for the cells of the Mark I battery. Two FeS_2 cells, M-1 and M-2, are also presented in this figure because they had previously shown specific energies at or near these goals.

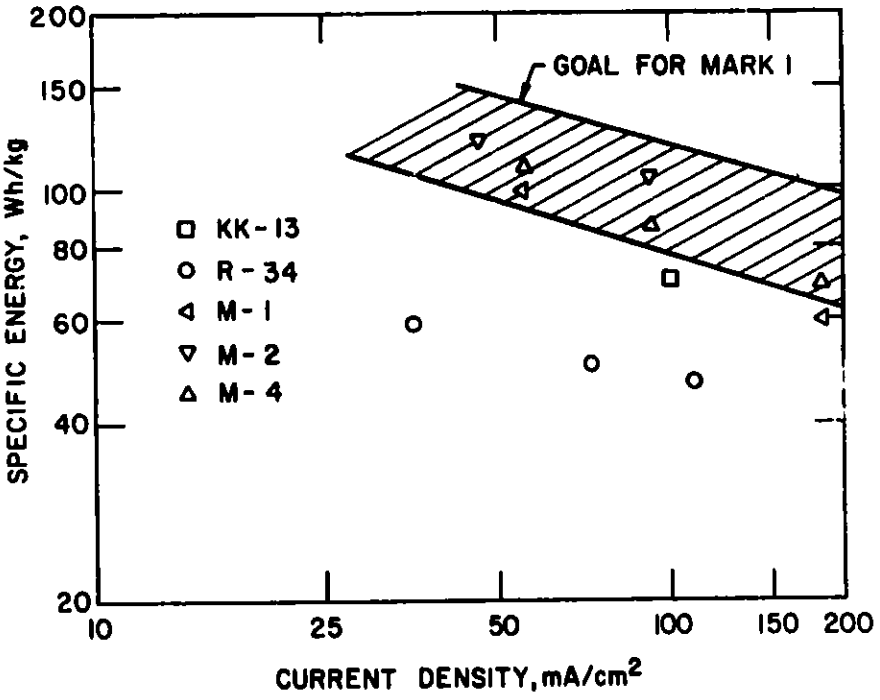

Fig. IV-2. Specific Energy as a Function of Current Density of Selected ANL Cells

As can be seen from this figure, Cell M-4 has reached the specific energy goal for the Mark I cell, and Cell KK-13 is close to the goal. Cell R-34 showed good specific energy at low-to-moderate current density (<100 mA/cm^2). An improvement in the specific energy of 20-30% is expected when an optimized version of this cell is completed.

V. MATERIALS DEVELOPMENT
(J. E. Battles)

Efforts in the materials program are directed toward the development of various cell components (electrode separators, current collectors, and cell hardware), testing and evaluation of cell materials (corrosion and wettability testing), and post-test examinations of cells to evaluate the behavior of the electrode and construction materials.

A. Electrode Separator Development
(R. B. Swaroop and C. W. Boquist)

Felt, powder, and paper separators are being developed as alternatives to the BN fabric currently used in Li-Al/FeS_x cells. These candidate separators will be less expensive and technically superior to the BN fabric.

1. In-Cell Testing

An additional batch of BN felt was received from Carborundum Co. The measured burst strength of these felts was 5-10 kPa, which is a great improvement over the more fragile felts received from Carborundum about nine months ago. These felts were also much easier to handle in subsequent cell construction. The porosity of the felts was between 90 and 93%, the thickness was 1.4 to 1.5 mm, and the areal density varied from 21 to 23 mg/cm^2. The as-received felts were stabilized by exposure to nitrogen gas at 1750°C. Cell SC-25 was constructed in a design identical to that of SC-19 (ANL-77-75, p. 34). This cell has a single layer of the stabilized BN felt* (1.25-mm thick) between the electrode frames, and has operated for 1050 hr and 70 cycles. The performance of this cell so far has been the best of the FeS test cells operated at ANL using BN felt separators. A detailed analysis of the performance of Cell SC-25 will be reported later.

Operation of Cell SC-21, which had a MgO powder separator, was terminated after 80 days and 131 cycles because of a gradually developing short circuit. As shown in Fig. V-1, the utilization of Cell SC-21 was poorer than that of Cell SC-19 or Cell SC-25, especially at high current densities. Post-test examination showed that, although the MgO did not react with other cell components, the thickness of the MgO layer was nonuniform on both sides of the positive electrode. In the area of the short circuit, the MgO layer was only 0.6 mm thick (original thickness, 1.8 mm). The short circuit occurred via intrusion of material from the positive electrode through the porous packing of the coarse MgO particles (-60 +120 mesh). The bulk packing density of the powder was apparently insufficient at the time of construction to prevent particle flow from the electrode to the separator. A similar cell using approximately 20 wt % fine (-120 mesh) MgO powder with the coarse MgO powder will be constructed so that a uniform powder layer can be obtained between the two electrodes.

*Cell SC-19 had a double layer (2.8-mm thick) of BN felt.

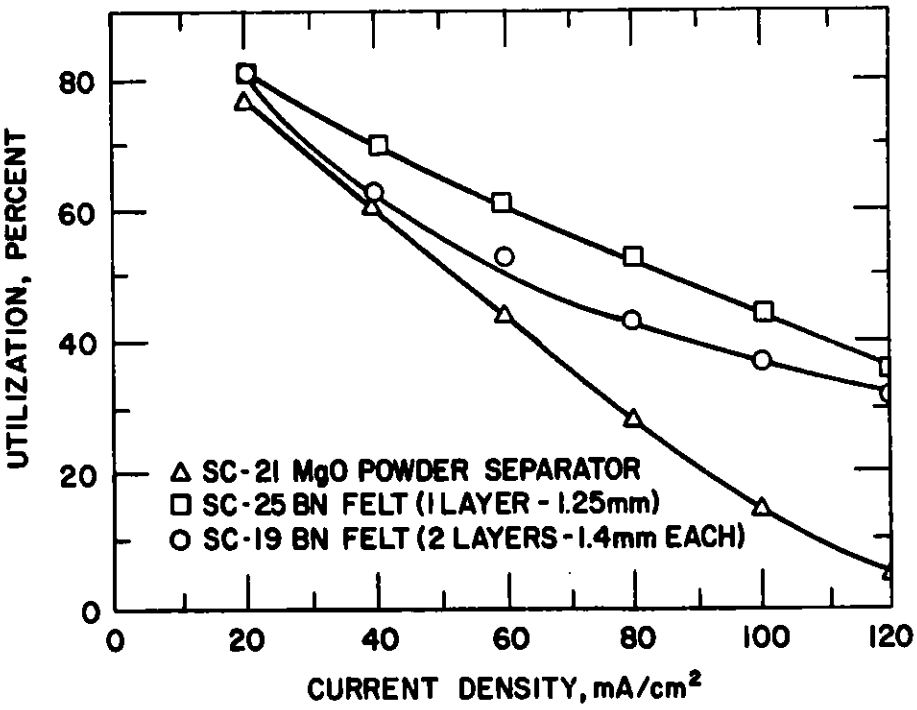

Fig. V-1. Utilization of Positive Material *vs.* Current Density for Three Test Cells (SC-19, -21, -25)

2. Out-of-Cell Testing

Study is continuing on the flowability (or creep behavior) of powder separators as well as electrode material-powder separator composites. Four specimens were investigated in a modified static-creep apparatus (ANL-77-75, p. 37): two were pellets of MgO powder (hot-pressed) and the other two were composites of MgO powder and FeS powder (one hot-pressed and the other cold-pressed). The results, summarized in Table V-1, indicate an initial creep of no more than 0.13% in the two MgO powder pellets during the first 200 hr of operation. The cold-pressed MgO-FeS composite underwent a deformation of 68% at 355°C, which is slightly above the melting point of the electrolyte (352°C). At this temperature the specimen deformed instantaneously. Upon termination of the tests, both the MgO and FeS were observed to have undergone extensive deformation. The hot-pressed MgO-FeS composite did not show such behavior, even up to 450°C, but underwent a deformation of approximately 3% (*i.e.*, almost 25 times more than the MgO powder specimens). Post-test examination of this hot-pressed composite showed that the FeS also flowed in a direction perpendicular to the applied load. The values of the thermal expansion coefficient for each specimen between room temperature and 350°C, also given in Table V-1, range between 9×10^{-6} and 17×10^{-6} per °C.

The preliminary conclusions of these out-of-cell studies are that (1) a MgO powder separator of 70 vol % solid will hold its shape after some initial degree of compaction, and (2) cold-pressed or hot-pressed FeS electrodes (50 vol % solids) will easily flow, swell, or shrink under stresses as low as 700 kPa. The minimum stress required to extrude FeS particles in composite specimens will be determined in future studies.

Table V-1. Thermal Creep Measurements on MgO and MgO-FeS Specimens

Specimen Composition, Volume %	Thickness, mm	Thermal Expansion Coefficient,[a] per °C	Creep Rate,[b] m/m per hr	Total Creep,[c] %	Remarks
71% MgO + 29% Salt	10.7	9×10^{-6}	7×10^{-6}	0.13	Creep in 140 hr
70% MgO + 30% Salt	10.6	13.5×10^{-6}	5.6×10^{-6}	0.06	Creep in 70 hr
50% (MgO-FeS) + 50% Salt[d]	12.0	17.4×10^{-6}	--	68	Instantaneous flow at 350°C. MgO and FeS both crept extensively.
70% (MgO-FeS) + 30% Salt	12.0	12.3×10^{-6}	103×10^{-6}	3	Only FeS crept (in 240 hr)

[a]Between room temperature and 350°C in helium environment.

[b]At 450°C under a static compressive stress of 700 kPa in helium environment.

[c]Percent of original thickness.

[d]This specimen was formed by cold-pressing; the other three were hot-pressed.

B. Ceramic Materials Development
(T. D. Claar and J. T. Dusek)*

This effort is concerned with three different tasks: (1) development of techniques for fabrication of rigid, porous separators; (2) development of electrically conductive ceramic coatings for positive current collectors; and (3) development of a technique for loading active material into porous metal structures. The first task is a continuing effort from FY 1977, whereas the latter two tasks were recently initiated.

1. Porous, Rigid Separators

Porous Y_2O_3 separators were fabricated using the plaster technique described in ANL-77-75, p. 39. Thin, rectangular plates (9 x 12 cm, 2 to 3-mm thick) were cast by pouring a Y_2O_3 and nitric acid slurry onto a flat stainless steel plate with raised edges made of plastic. Within about 10-20 min after casting, the slurry set to a firm plaster, which was dried overnight at room temperature on the steel plate. The thickness of the plaster was determined by the height of the raised edges. The cast separators were then carefully removed from the steel plate and placed in a vacuum drying oven, where they were heated to 150-170°C over a period of about 8 hr and dried overnight. After this drying cycle, the separators were fired in air at 1500°C for 12-15 hr in a Globar furnace to obtain a partially sintered microstructure.

A number of Y_2O_3 plates were fabricated by this technique. The following parameters were varied in the preparation of these materials: (1) concentration of the nitric acid solution, (2) ratio of Y_2O_3 powder-to-acid solution, (3) duration of the wetting and stirring steps during preparation of the slurry, and (4) firing schedule.

For the Y_2O_3 powder† used in these studies, the following procedure yielded porous plates of reproducible quality that were free from cracks and warpage after drying: (1) pour 50 g of Y_2O_3 powder into a glass beaker containing 50 cm^3 of 1 nitric acid, (2) allow the nitric acid to wet and react with the Y_2O_3 particles by soaking for 1.5 min, (3) moderately mix slurry with spatula for 2 min and then pour this mixture onto the plates with raised edges, and (4) follow the procedure given in the first paragraph.

Higher concentrations of nitric acid (2-3 *M vs* 1 *M*) produced plates of somewhat higher dried strength, but decreased the allowable working time. The working time was also decreased with increasing powder-to-acid ratios. Plates made from 2 *M* acid were stronger after firing at 1500°C than similar ones made from 1 *M* solution, and the soaking and mixing periods were reduced to 0.5 min and 1.75 min, respectively.

---

*Materials Science Division of ANL.

†As-received 99.99% Y_2O_3 manufactured by Molycorp. Inc., White Plains, NY.

Significant effects on microstructure and bending strength were observed when two Y_2O_3 plates (designated 59C and 59E) made with 1 *M* nitric acid were sintered at different temperatures. Both plates were fired at 1500°C in air for 15 hr, and plate 59C was given an additional firing at 1800°C in vacuum for 2 hr. This firing at 1800°C resulted in a significant increase in bending strength because of the higher degree of sintering, as shown in Fig. V-2. The porosities of plates 59E and 59C were estimated to be 70 and 55 vol %, respectively.

The most significant problem associated with the plaster technique appears to be warpage resulting from the large linear shrinkages (20-25%) that occur during firing. Attempts are being made to minimize this problem by determining the effects of Y_2O_3 powder reactivity, plate thickness, and firing technique. Porous Y_2O_3 separators prepared by this casting technique are expected to be available for in-cell testing during the next quarter.

2. Ceramic Coatings for Positive Current Collectors

Electrically conductive ceramic coatings on inexpensive metallic substrates are being investigated for use as positive current collectors. The requirements of a ceramic-coated current collector include: (1) sufficient electronic conductivity to provide adequate collection efficiency, (2) resistance to corrosion in the environment of FeS_2 and LiCl-KCl at 450°C, (3) resistance to spalling under mechanical and thermal stresses, and (4) lower cost than the molybdenum current collectors now used in FeS_2 cells.

Selected properties of some transition metal borides, carbides, and nitrides were reviewed. Electrical resistivities of these materials generally range from 10 to 200 μΩ-cm at room temperature; the borides generally have lower resistivities than the corresponding metal nitride and carbide compounds.

The chemical stabilities of the borides, carbides, and nitrides of niobium, tantalum, titanium, and zirconium with respect to formation of the metal sulfides at 427°C were evaluated by calculation of the free-energy changes associated with the sulfidation reaction. These calculations indicated that TiB_2 is stable in the positive electrode environment at 427°C if the boron activity is greater than 0.3, and that TiN is stable in this same environment if the nitrogen activity is equivalent to a nitrogen partial pressure $\geq 6 \times 10^{-6}$ atm. Other candidates for current-collector coatings will be identified by a similar thermodynamic approach as well as by static corrosion testing.

Contacts are being established with commercial vendors who have experience in the application of inorganic coatings by chemical vapor deposition, ion plating, sputtering, plasma spraying, and diffusion. Candidate coating materials procured from these industrial firms will be examined and tested using a variety of techniques. Coating materials showing the best overall performance in static corrosion tests will be further developed and then tested in operating cells.

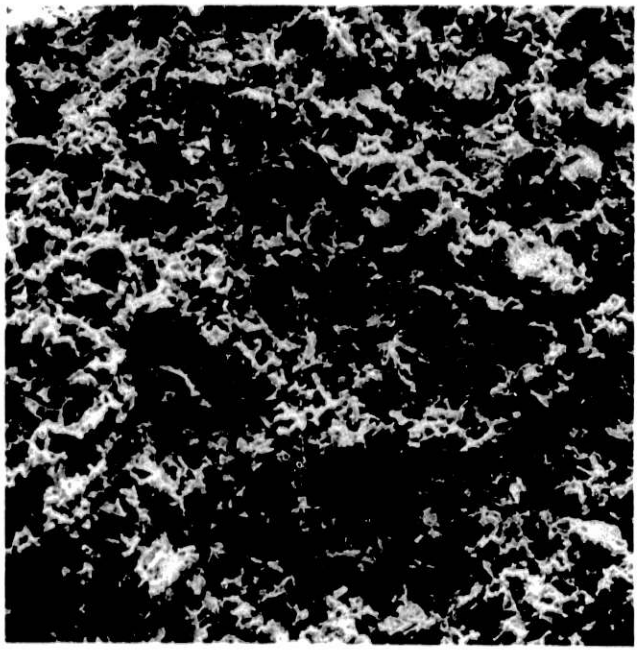

(a) 600X

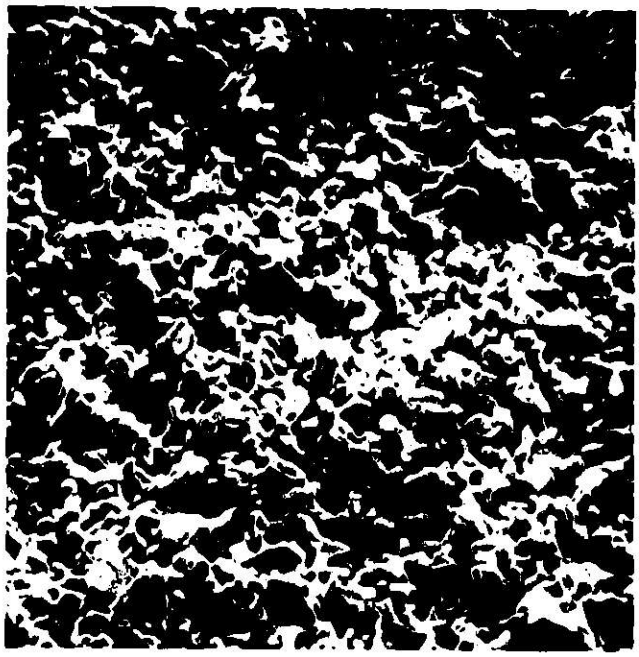

(b) 600X

Fig. V-2. Scanning Electron Micrographs of Porous Y_2O_3 Separator Plates Formed from 1 *M* Nitric Acid and Y_2O_3 Powder.
(a) Specimen 59E--Fired for 15 h at 1500°C.
(b) Specimen 59C--Fired for 15 h at 1500°C and 2 h at 1800°C.

3. Loading of Electrode Material

A study has been initiated to determine the most effective means of loading powdered active materials into porous metal structures such as Foametal and Retimet.* Preliminary experiments on the vibratory loading of aluminum powder into Retimet structures have been completed. The effects of particle size of the aluminum powder and the pore size of the Retimet on the packing densities were determined by weight measurements. The goal for the amount of aluminum powder packed into a Retimet structure is 65-70 vol %.

Samples of iron and nickel Retimet having coarse, intermediate, and fine pore distributions were quartered into 7.6-cm squares (0.7-cm thick); the volume of the porous metal body was approximately 40 cm^3. These Retimet materials have a nominal porosity of 95 vol %, and the open-cell structure of these materials consists of a highly sintered metal network surrounding 0.2- to 2.5-mm-dia voids with roughly spherical geometries.

As-received Alcoa aluminum powder was loaded into the above Retimet squares using a Syntron Model PJ-15 vibratory table. The aluminum powder had particle sizes ranging from +60 mesh (>250 μm) to -325 mesh (<44 μm); approximately 90 wt % of the particles were nearly equally divided among three size fractions: +60, -60 +100, and -100 +200 mesh. The packing density of as-received aluminum powder ranged from 52.9 vol % for coarse nickel Retimet to 43.6 vol % for the fine iron Retimet.

The effect of particle size distribution on packing density was determined by vibrating various size fractions of aluminum powder into iron structures with fine pore sizes. The maximum packing density was 45.7 vol % for the -100 +200 mesh aluminum powder.

Tests indicated that vibratory loading of aluminum powder in the form of a slurry leads to increased packing densities. In one experiment, dry powder (-60 mesh) was vibrated to a packing density of 42 vol %. After adding methanol, additional powder could be vibrated into place to achieve a packing density of 53 vol %. Further investigations of this methanol slurry technique of vibratory loading are planned. Methods of retaining the loaded particles in the Retimet structures and techniques other than vibratory loading will also be studied.

Preliminary work has been initiated on the packing of FeS_2 powder to a density of approximately 30 vol %.

C. Cell Wetting Studies
(J. G. Eberhart)

The internal resistance of a lithium-aluminum/iron sulfide cell is determined in part by the extent to which the molten LiCl-KCl electrolyte fills the pores of the two electrodes and the separator. Pore filling is, in turn, a function of the wettability of the electrode and separator structures by the electrolyte. Thus, experiments are in progress to identify the factors which influence wettability of separator and electrode materials and to explore possible means of improving their wettability.

*Manufactured by Dunlop Limited, Coventry, England.

Contact-angle measurements were made with molten LiCl-KCl electrolyte on positive and negative electrode materials. The determinations were made at 400°C in a helium-atmosphere glove box. On a surface of FeS_2 (representing a charged positive electrode) the advancing and receding contact angles are 147° and 38°, respectively. On surfaces of iron and Li_2S (representing a discharged positive electrode) the advancing contact angle is 106° for iron and 116° for Li_2S and the receding contact angle is 60° for iron and 64° for Li_2S. The maximum contact-angle ranges for these surfaces are shown in Fig. V-3, along with data previously obtained for BN and Type 304 stainless

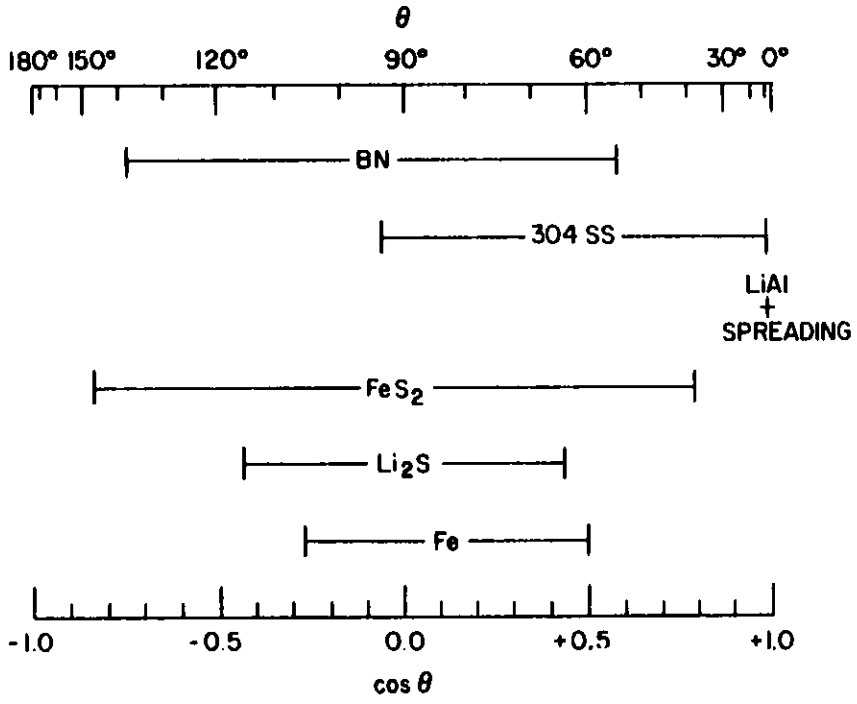

Fig. V-3. Maximum Electrolyte Contact Angle Ranges for Various Cell Components

steel. All of these materials have advancing angles which are greater than 90° and receding angles which are less than 90° (*i.e.*, difficult to penetrate). Thus, pressed powder structures of any of the above materials are not expected to be spontaneously wet with electrolyte. The application of force will be required to achieve penetration of these materials by the electrolyte. This can be accomplished through evacuation and repressurization of the cell or through a hot-pressing operation.

Contact-angle measurements were also made on a surface of Al-17.5 wt % Li (representing a charged negative electrode) and Al-12.0 wt % Li (representing a partially discharged electrode). Within 10-15 min the electrolyte spreads on both surfaces. The "equilibrium wettability"* of LiAl

*The contact angle for salt on LiAl changes with time for about 10 min, finally approaching θ=0°. The equilibrium θ is the final steady value.

is also shown in Fig. V-3. If the electrolyte also spreads on LiAl which is further depleted in lithium, then no wetting problems are expected in the negative electrode.

Efforts are continuing to find methods of pretreating BN separators that improve their wettability and are easily adaptable to manufacturing procedures. One pretreating method* has been tested successfully. Boron nitride felt was "dusted" with a fine powder of $LiAlCl_4$ (mp, ~142°C); the treated felt was then easily penetrated by molten LiCl-KCl electrolyte without having to resort to evacuation and repressurization of the system. Further tests are planned to determine the minimum amount of $LiAlCl_4$ required to produce this change in separator wettability and to test various methods for applying the powder.

Work is continuing on a procedure for prewetting of separators with molten electrolyte before cell assembly (ANL-77-75, p. 42). Steel frames that hold the separator in place have been fabricated for this procedure. A container for immersing the separator in molten electrolyte has been assembled† with a prismatic shape to conserve electrolyte. Several (13 x 13 cm and 13 x 18 cm) BN separators will be prepared to test this procedure. These separators will then be available for in-cell tests.

D. Post-Test Cell Examinations

(F. C. Mrazek, N. C. Otto, J. E. Battles)

Post-test examinations are conducted both on small experimental cells‡ and on engineering-scale cells.** The objectives of these examinations are to determine (1) morphological effects (*e.g.*, electrode microstructure, distribution and utilization of active material, reaction uniformity, electrode swelling, impurities, and cross-contamination of electrodes), (2) in-cell corrosion reactions and reaction rates, and (3) the causes of cell failure. These results are evaluated, and appropriate recommendations are made for improved cell designs.

1. Carbon Analyses of Negative Electrodes

Carbon analyses†† were conducted on the negative electrodes from three engineering-scale cells with positive electrodes that were either carbon-bonded or contained added carbon (Cells KK-4, KK-5, and PC-2-01). The results, listed in Table V-2, indicate that a significant amount of carbon had migrated from the positive electrode. Two carbon analyses of the present supply of as-received and filtered Lithcoa electrolyte showed only

---

*Suggested by J. E. Battles.

†P. F. Eshman.

‡Fabricated and tested at ANL.

**Fabricated either at ANL or an industrial firm and operated at ANL.

††I. M. Fox, Analytical Chemistry Laboratory.

Table V-2. Carbon Analysis of Negative Electrodes

Cell No.	Operation time, days	Carbon, wt %
KK-4[a]	208	0.16, 0.25
KK-5[a]	340	0.24, 0.28[b] 0.21, 0.21[c]
PC-2-01[d]	31	0.07, 0.08

[a]Visual inspection of the initial supply of electrolyte used in these cells indicated minor amounts of carbon particles in electrolyte. Not analyzed.

[b]These values determined at front of the electrode, *i.e.*, the face nearest the positive electrode.

[c]These values determined at back of the electrode.

[d]This cell had pellet positive electrodes with carbon additive; the other two cells had carbon-bonded positive electrodes.

40 and 30 ppm, respectively. The effect (if any) that carbon in the negative electrode (or separator) has on cell performance is unknown at this time. The extent of carbon migration is suspected to depend on the amount of carbon added to the positive electrode and the operating time of the cell.

2. Formation of Y_2O_2S in Y_2O_3 Separators

Post-test examinations of Y_2O_3 separators (both felt and powder) from FeS_2 cells have shown evidence of sulfur reaction with the Y_2O_3. The reaction product was identified as Y_2O_2S by X-ray diffraction* and scanning electron microscopy. This yttrium oxysulfide has also been identified in an FeS cell that was operated for 83 days. Examinations of three other FeS cells with Y_2O_3 separators that had operated for shorter periods of time showed no evidence of Y_2O_2S. In FeS_2 cells with Y_2O_3 separators, Y_2O_2S was identified in two cells that had operated for less than 42 days. The formation of Y_2O_2S leads to reduced cell performance through loss of sulfur in the positive electrode and through reduced porosity of the separator. These results indicate that Y_2O_3 may be unsatisfactory as a separator material.

*B. S. Tani, Analytical Chemistry Laboratory.

3. Lithium Gradient in Negative Electrodes

As previously reported (ANL-77-35, p. 44), metallographic and chemical analyses indicate that a significant lithium concentration gradient occurs in charged Li-Al electrodes. This observation was confirmed by ion microprobe analysis. A plot of the probe results is shown in Fig. V-4 for three cells: Cells LT-2 (totally charged and discharged), EP-I-6-A-1 (fully charged), and G-04-008A (about 50% charged). The thickness of the electrodes is indicated by the end-point of the curves. In Cell LT-2, the lithium was cycled between two aluminum electrodes so that at full charge one electrode would be LiAl while the other would be aluminum. The curves should be considered as an indication of the trend in the lithium concentration gradient rather than as quantitative results, because of the large scatter in the data. Efforts are under way to improve the accuracy of the data. The electrodes from cells EP-I-6-A-1 and LT-2 in the fully charged state show a very steep lithium gradient. The 50% charged electrode from Cell G-04-008A shows a lesser gradient. The data on this electrode showed a larger scatter than the data from the other two electrodes, which was attributed to a greater degree of lithium nonuniformity within a given Li-Al particle. This nonuniformity is probably the result of the cell's short operating time and its having been assembled in an uncharged state.

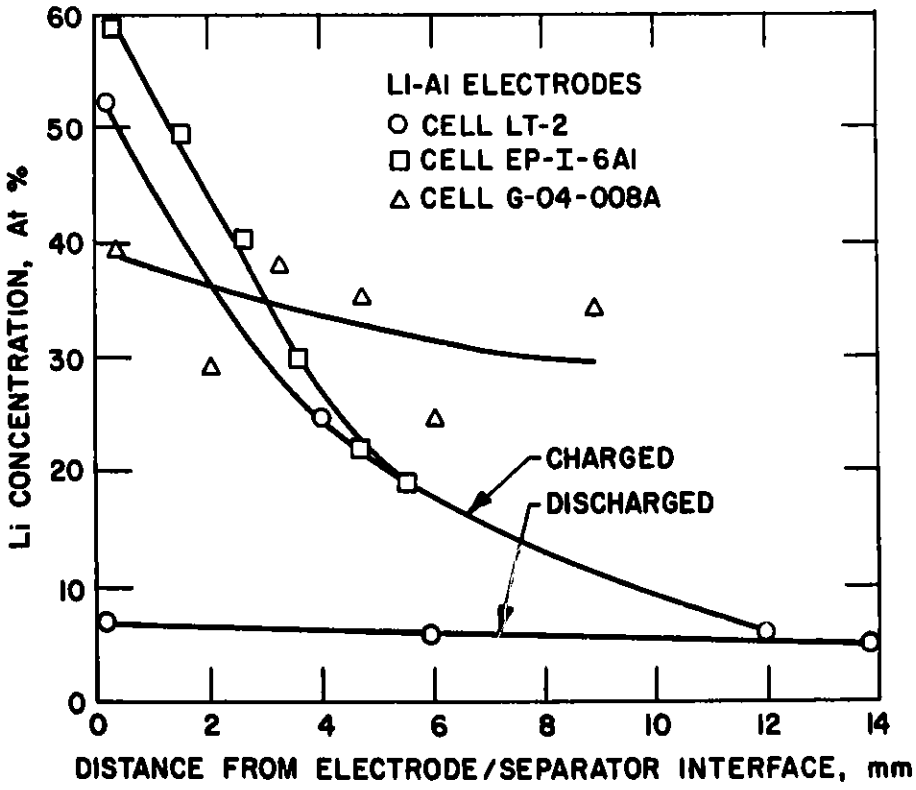

Fig. V-4. Lithium Concentration Profiles in the Negative Electrodes of Three Cells

4. Causes of Cell Failure

During this quarter, a total of 20 vertical, prismatic engineering cells were examined to determine the cause of failure, and the results of these examinations are shown in Table V-3. (A cell whose operation was terminated at the end of testing, *i.e.*, no failure, was also examined.)

Table V-3. Cell Failure Mechanisms

Cause of Failure	Cases	
	This Period	Overall[a]
Extrusion of electrode material	2	20
Metallic Cu in separator[b]	1	11
Separator cut by honeycomb current collector	8	17
Equipment malfunction[c]	0	7
Short in feedthrough	1	4
Improper cell assembly	3	5
Broken positive conductor	0	2
Unidentified		
Declining performance[d]	3	10
Short circuits	1	4

[a]This includes all vertical, prismatic cells that have undergone post-test examinations to date.

[b]FeS cells only.

[c]Overcharge, temperature excursion, or polarity reversal.

[d]Generally indicative of early stages of short circuit.

Cell failure mechanisms for all of the cells examined to date (81 cells) are also included in Table V-3. The major cause of cell failure during this quarter was the cutting of separators by the honeycomb current collector of the positive electrode. Cells are now being fabricated with protective screens (as recommended), which should eliminate this problem in the future. Three cases of failure from improper cell assembly were also identified. Two of these failures were caused by the ZrO_2 cloth (which becomes conductive as it reacts with lithium) contacting both the positive and negative electrodes. The third failure was caused by a mechanical misalignment of the positive electrode in cell assembly. Isolated defects in the BN fabric separator caused by improper handling or weaving are believed to be the major cause of failure from unidentified short circuits, and is perhaps also a factor in unidentified declining efficiency.

VI. CELL CHEMISTRY
(M. F. Roche)

The cell chemistry group (1) investigates specific chemical and electrochemical problems that arise in the development of cells and batteries, (2) conducts studies that are expected to lead to improvements in electrodes, electrolyte, and other cell components, as well as to provide a basic understanding of the processes that occur within cells.

A. Properties of FeS_2 Electrodes

1. The Li-Fe-S Phase Diagram
(A. E. Martin)

The region of the Li-Fe-S phase diagram that is of interest in the operation of lithium/metal sulfide cells is the Li_2S-FeS_2-Fe triangle. This region of the phase diagram has been studied in a variety of in-cell and out-of-cell tests at cell operating temperatures (see, for example, ANL-77-75, pp. 49-50). The results of these studies are presented in Fig. VI-1.

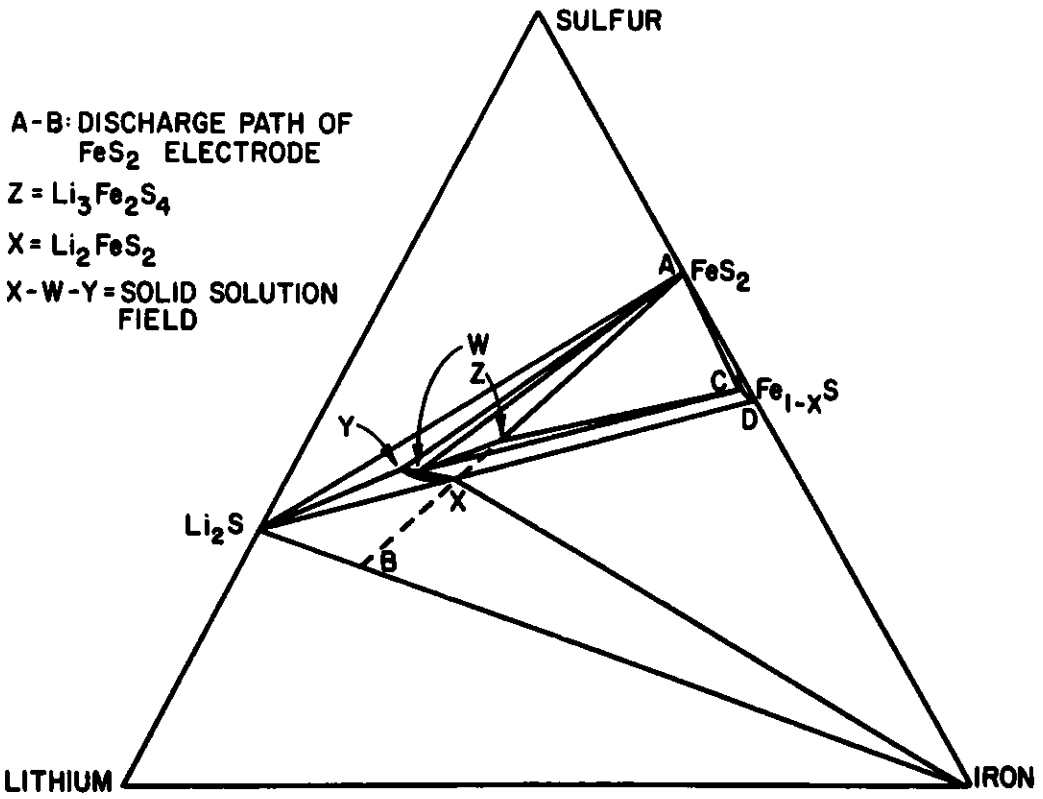

Fig. VI-1. Isothermal Section of Li-Fe-S Phase Diagram at 450°C Showing the Charge-Discharge Path of FeS_2 Electrodes

The path representing the change in average composition of an FeS_2 electrode as it is charged and discharged at 450°C is indicated by the line A-B. The fully charged electrode contains FeS_2 (point A) and the fully discharged electrode contains Li_2S and iron (point B). Between these extremes, two well-defined compounds are found on the line A-B, namely, Z phase ($Li_3Fe_2S_4$) and X phase (Li_2FeS_2). In addition, more complex phases occur in the region between Z and X phase (*e.g.*, mixtures of the compounds $Fe_{1-x}S$, W, and Z).

The in-cell behavior of FeS_2 electrodes can be described with the aid of Fig. VI-1. During discharge, FeS_2 is converted to Z phase. Next, Z phase is converted to a mixture of the compounds $Fe_{1-x}S$ and W. The latter compound lies on the boundary of a solid-solution field labeled X-Y. The extent of this solid solution field and the approximate location of the W compound on the field boundary are indicated in the figure. Further discharge of the compounds $Fe_{1-x}S$ and W leads to formation of the single-phase compound, X phase. Finally, X phase is discharged to a mixture of Li_2S and iron.

During charge, Li_2S and iron form X phase, and X phase is then converted to a mixture of the compounds $Fe_{1-x}S$ and W. At this stage, the charge mechanism differs from the discharge mechanism. Although some Z phase is known to form during charge of the mixture of W and $Fe_{1-x}S$ (*i.e.*, the reverse of the discharge reaction), the favored reaction appears to be formation of FeS_2 on the surface of $Fe_{1-x}S$ particles by solution transport of some electrolyte-soluble, sulfur-rich species (ANL-77-68, p. 49 and ANL-77-75, p. 49). This reaction occurs at about the potential required for generation of sulfur from Li_2S (ANL-77-68, p. 48).

In the positive electrode, solid phases other than those shown on the Li-Fe-S ternary diagram can exist because of the presence of LiCl-KCl electrolyte. One such phase is J phase ($LiK_6Fe_{24}S_{26}Cl$), which plays a major role in the operation of FeS electrodes (ANL-77-17, p. 42). Another is $KFeS_2$, which forms in FeS_2 electrodes with KCl-rich electrolyte (see Section VI.A.2.).

2. Cyclic Voltammetry of FeS_2 Electrodes
(S. K. Preto, C. C. Sy, M. F. Roche)

In a recent Li-Al/FeS_2 cell test in which only one-third of the FeS_2 capacity was utilized, the cell reaction exhibited good electrochemical reversibility (ANL-77-75, p. 55). The discharge reaction in this cell was the high-voltage (1.74 V) reaction of FeS_2:

$$2FeS_2 + 3LiAl \rightarrow Li_3Fe_2S_4 \text{ (Z phase)} + 3Al$$

The good reversibility exhibited by this cell indicated that the charge reaction was the reverse of this discharge reaction. Earlier voltammetry studies (ANL-77-68, p. 46) showed that the high-voltage reaction of FeS_2 had poor electrochemical reversibility when the FeS_2 capacity was fully utilized. The FeS_2 voltammogram given in Fig. VI-2 illustrates this effect (charge reactions are shown above the horizontal line and discharge reactions

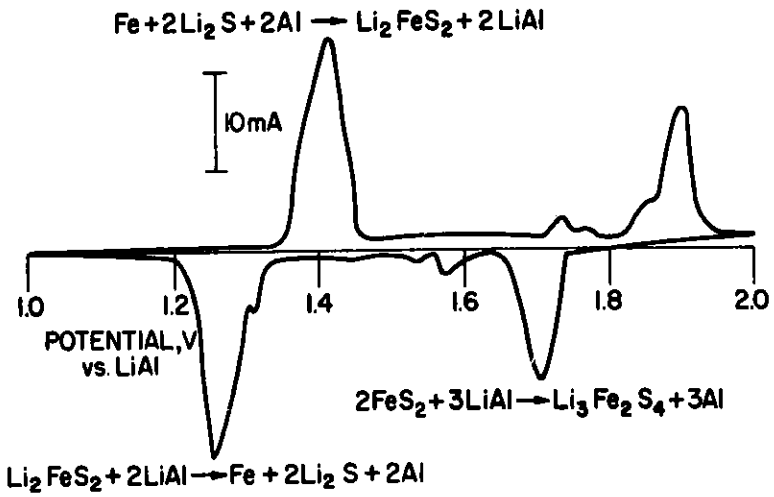

Fig. VI-2. Cyclic Voltammogram of FeS_2 Electrode in LiCl-KCl Electrolyte of Eutectic Composition

below). Poor electrochemical reversibility is indicated by the large voltage separation between the major charge and discharge reactions in the high-voltage region (1.5 to 2.0 V). The charge reaction in this voltage region has been attributed to formation of an electrolyte-soluble, sulfur-rich species. These results suggest that the voltage of this charge reaction depends on the electrode utilization. This possibility was examined in the present voltammetry tests by varying the discharge cutoff voltage. Electrolyte effects were also studied by varying the LiCl-to-KCl ratio.

In this study, an FeS_2 working electrode (116 mg of FeS_2 in carbon foam within a molybdenum housing) was cycled at 400°C *vs.* LiAl reference and counter electrodes. The voltage scan rate was 0.02 mV/sec. Electrolyte variations were accomplished by adding either LiCl or KCl to 58 mol % LiCl-42 mol % KCl eutectic* in order to shift the composition to 61 mol % LiCl-39 mol % KCl or 55 mol % LiCl-45 mol % KCl. During the tests, the electrolyte was occasionally shifted back to eutectic composition, and scans were made to check for recovery of the electrode to its "normal" irreversible behavior (Fig. VI-2). The voltage range was changed in each voltammogram by varying the discharge cutoff voltage,† as shown in Fig. VI-3.‡ For the FeS_2 voltammogram in LiCl-rich electrolyte, the discharge cutoff voltages were 1.65, 1.61, 1.56, and 1.43 V. Although not shown in Fig. VI-3, sweeps were also taken of FeS_2 in this electrolyte to a 1.35-V

*Supplied by Anderson Physics Laboratory, Champaign, IL.

†In all cases, a significant number of scans were obtained after changing conditions to insure that the electrodes and electrolyte had reached a steady state.

‡No great significance should be attached to differences in peak areas. The electrode was operated for 500 hr; during this time the capacity declined by 40%. The peaks differ in area because the sweeps were obtained at different times.

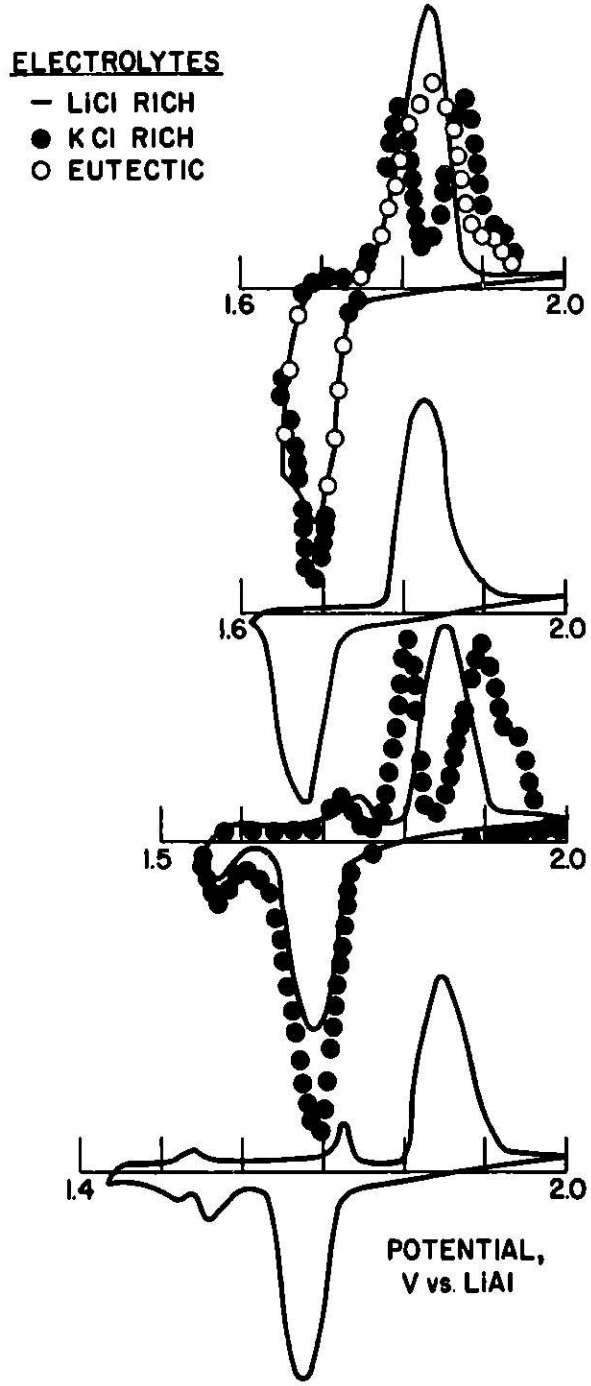

Fig. VI-3. Cyclic Voltammograms of FeS_2 Electrode in LiC-KCl Electrolyte of Varying Compositions (Discharge Cutoff Voltages from Top to Bottom: 1.65, 1.61, 1.56, 1.43 V)

cutoff and a 1.0-V cutoff. Study of this figure led to the observation that, as the discharge cutoff voltage is lowered, the left side of the major charge peak shifts up scale and the right side of the discharge peak remains fixed. The separation of the charge and discharge reactions is less than 20 mV with a 1.65-V cutoff; however, the separation is about 90 mV with a 1.43-V cutoff (the separation with the 1.0-V and 1.35-V cutoff is about the same as that of the 1.43-V cutoff). The good reversibility observed with a 1.65-V cutoff indicates that the reaction $2FeS_2 + 3LiAl \rightarrow Li_3Fe_2S_4 + 3Al$ is electrochemically reversible; this is in agreement with the cell test described at the beginning of the section. The poorer reversibility observed with lower cutoff voltages indicates that the discharge of $Li_3Fe_2S_4$ is the reaction with poor reversibility. The products of the irreversible discharge of $Li_3Fe_2S_4$ are the compounds $Fe_{1-x}S$ and W. Apparently, the kinetically hindered step during charge is the recombination of these compounds to form $Li_3Fe_2S_4$.

The dotted curves in Fig. VI-3 show the behavior of FeS_2 in KCl-rich electrolyte. Two tentative conclusions can be drawn from these curves. First, the discharge reaction is essentially the same in LiCl-rich and KCl-rich electrolyte because the position of the discharge peak is identical in both electrolytes. Second, the charge reactions are different in the two electrolytes. In the case of the KCl-rich electrolyte, the high-voltage charge reactions do not appear to change significantly with shifts in discharge cutoff voltage; the high-voltage charge reactions consist of a narrow peak that begins at about 1.74 V and a poorly resolved doublet that begins at about 1.84 V. The area of the doublet is about twice that of the narrow peak, and the sum of these areas is equal to the area of the discharge peak. (The same features are seen with a discharge cutoff voltage as low as 1.0 V). Because this type of behavior was only observed in KCl-rich electrolyte, a potassium-containing sulfide phase was suspected.

For an FeS_2 cell using KCl-rich electrolyte the proposed reactions consistent with the above observations are as follows:

Discharge:* $2FeS_2 + 3LiAl \xrightarrow{3e^-} Li_3Fe_2S_4 + 3Al$, ∿1.74 V

Charge: a) $Li_3Fe_2S_4 + 2KCl + Al \xrightarrow{1e^-} 2KFeS_2 + 2LiCl + LiAl$, ∿1.74 V

b) $2KFeS_2 + 2LiCl + 2Al \xrightarrow{2e^-} 2FeS_2 + 2KCl + 2LiAl$, ∿1.84 V

a+b) $Li_3Fe_2S_4 + 3Al \xrightarrow{3e^-} 2FeS_2 + 3LiAl$

A combination of metallographic studies and X-ray analyses have now shown that $KFeS_2$ is a major phase in FeS_2 electrodes operated in KCl-rich electrolyte (see Section VI.A.3.). This supports the proposed reaction mechanism.

*The absence of a potassium-containing intermediate in this discharge step suggests that the reverse of charge reaction (b) is electrochemically hindered.

As can be seen in the upper voltammogram in Fig. VI-3, a mixture of the electrode behavior in LiCl-rich and KCl-rich electrolyte occurs in the electrode with eutectic electrolyte. In similar fashion to the high-voltage reaction of FeS_2 in LiCl-rich electrolyte, the high-voltage reaction of the FeS_2 in eutectic electolyte ($Li_3Fe_2S_4 \leftrightarrows FeS_2$) is reversible.

The FeS_2 reactions were also examined in LiF-LiCl-LiBr* at 460°C in order to eliminate all possible potassium-ion effects. The discharge peak was shifted to a higher voltage, about 1.77 V, because of the high temperature required with this electrolyte. This shift, which is also observed in LiCl-KCl at high temperatures, is associated with the higher sulfur activity of the positive electrode at higher temperatures. The charge peaks in the high-voltage region were identical to those in LiCl-rich electrolyte. The identical charge peaks indicate that the kinetically hindered formation of $Li_3Fe_2S_4$ from the compounds $Fe_{1-x}S$ and W is not due to potassium ion effects in LiCl-rich or eutectic LiCl-KCl electrolyte.

The conclusions from the above tests are: 1) the formation of $Li_3Fe_2S_4$ from its discharge products ($Fe_{1-x}S$ and W) is electrochemically hindered in LiCl-rich or eutectic LiCl-KCl electrolyte; and 2) in KCl-rich electrolyte, the electrode reactions are different than in LiCl-rich or eutectic LiCl-KCl electrolyte and involve a potassium-containing phase.

3. Formation of $KFeS_2$ in KCl-Rich Electrolyte

(A. E. Martin, Z. Tomczuk)

The voltammetry studies in the preceding section indicated that $KFeS_2$ would form during the charge of FeS_2 electrodes in KCl-rich electrolyte. To check this possibility, the chemical formation of $KFeS_2$ was studied. Mixtures of Li_2S and FeS_2 in three different electrolyte compositions were reacted at 525° under conditions that produce extensive amounts of $Li_3Fe_2S_4$ in eutectic salt. The first mixture contained LiCl-KCl eutectic salt, the second contained LiCl saturated with KCl, and the third contained KCl saturated with LiCl. Metallographic examination of the reaction products showed that the first and third products contained $Li_3Fe_2S_4$, and that the second mixture contained a new phase in addition to $Li_3Fe_2S_4$. The new phase was very similar in morphology to $Li_3Fe_2S_4$, but differed from it in color (pink instead of colorless) and in anisotropy (less anisotropic). The products of the three reactions were leached with water to dissolve the LiCl, KCl and $Li_3Fe_2S_4$. The residues were then examined by X-ray diffraction† and by metallography. The X-ray diffraction examination showed that $KFeS_2$ was present in the residue from the second reaction product, but not in the residues of the first or third. The metallographic examination showed that the pink phase was present in the second residue but not in the other residues. Thus the pink phase was established as $KFeS_2$.

---

*A high cost and high density make this electrolyte less satisfactory than LiCl-KCl for applications in FeS_2 cells.

†B. S. Tani, Analytical Chemistry Laboratory.

The positive electrode from a LiAl (2A-hr)/FeS_2 (1A-hr) cell also underwent testing. It was operated at 430°C in KCl-rich electrolyte, and operation was then terminated at 50% charge of the upper plateau. Upon post-test examination, an unreacted portion of the FeS_2 electrode was found to contain the original FeS_2 particles. In the well-reacted zone, the major phase was $KFeS_2$, and the minor phases were $Fe_{1-x}S$, $Li_3Fe_2S_4$, and FeS_2

4. The Form of Cobalt in FeS_2-CoS_2 Electrodes
(A. E. Martin)

Although CoS_2 has been employed as an additive for FeS_2 electrodes for some time, the identity of the cobalt-containing phases has not been established. The Co-S phase diagram of M. Hansen and K. Anderko[2] shows that Co, Co_9S_8, $Co_{1-x}S$, Co_3S_4 and CoS_2 exist at cell operating temperatures. In addition, Co, $Co_{1-x}S$, and CoS_2 are known to be capable of forming solid solutions with their iron analogs. Experiments were conducted to search for other interactions.

No metallographic evidence for the formation of Li-Co-S phases was detected when Li_2S, Co_9S_8 and $Co_{1-x}S$ were melted together. Melting of Li_2S, FeS and Co_9S_8 (5:4:1 mole ratio) produced Li_2FeS_2, Li_2S and Co_9S_8. Various mixtures of Li_2S with Co_9S_8, $Co_{1-x}S$, Co_3S_4 and CoS_2 in electrolyte at cell operating temperatures yielded no evidence for Li-Co-S phases, and no reactions were observed in a mixture of Li_2FeS_2, Co_9S_8, $Co_{1-x}S$ and electrolyte at cell operating temperatures. The above tests indicate that no cobalt analogs of Li_2FeS_2, $Li_3Fe_2S_4$, or J phase ($LiK_6Fe_{24}S_{26}Cl$) exist. Cobalt does not appear to be included in these iron compounds to any significant extent. Thus iron and cobalt sulfides in FeS_2 cells appear to follow independent discharge-charge paths; cobalt is only present as binary cobalt-sulfur compounds.

The original purpose of adding cobalt sulfide (ANL-75-1, p. 29) was to improve the electronic conduction of FeS_2 through the formation of solid solutions of iron-cobalt disulfides, which are metallic conductors. The above experiments suggest that solid solution formation of this type is not likely to occur in an FeS_2 cell to a significant extent. Therefore, a reassessment of the effects of this additive on cell performance should be undertaken.

5. Substitution of CsCl for KCl in the Electrolyte
(Z. Tomczuk)

A LiAl (2 A-hr)/LiCl (59 mol %)-CsCl (41 mol %)/FeS_2 (1A-hr) cell was operated at 433°C. The cell voltage curves during charge and dishcharge were similar to those of the LiAl/FeS_2 cell using LiCl-KCl electrolyte. Therefore, CsCl substitution for KCl does not improve cell performance.

B. Properties of MS and FeSe Electrodes

1. J Phase in FeS Electrodes
(Z. Tomczuk, S. K. Preto, A. E. Martin)

Slow-scan cyclic voltammetry of FeS *vs.* LiAl in LiCl-KCl eutectic at 430°C showed that the charge curve for this electrode consisted of two peaks of nearly equal size (ANL-77-35, p. 57). In this study, the charge reactions were believed to be:

$$Fe + 2Li_2S + 2Al \rightarrow Li_2FeS_2 + 2LiAl \qquad 1.350\ V$$

$$Fe + Li_2FeS_2 + 2Al \rightarrow 2FeS + 2LiAl \qquad 1.375\ V$$

The J phase ($LiK_6Fe_{24}S_{26}Cl$) was thought to occur as an intermediate phase during the second reaction and to convert to FeS by the end of the second reaction peak (1.42 V). However, cell data presented earlier (ANL-75-1, p. 103) indicated that the J-phase transition to FeS at 430°C did not occur below 1.60 V.

In order to determine whether or not a high potential is required for conversion of J phase to FeS, two additional LiAl (1 A-hr)/LiCl-KCl/FeS (2 A-hr) cells were operated at 400-410°C. These cells were cycled at a current density of 12 mA/cm^2 between 1.0 and 1.6 V. Operation of the first cell was terminated during a 12 mA/cm^2 charge at 1.50 V, and the positive electrode was rapidly removed. The second cell was charged at 12 mA/cm^2 to 1.50 V, and was then trickle-charged for four days at a constant voltage of 1.50 V and a current density of about 0.4 mA/cm^2 (probably the self-discharge rate at 1.50 V). At the end of this period, the electrolyte was frozen while the cell voltage was maintained at 1.50 V.

Metallographic examination showed that J phase was dominant in both of the electrodes. In fact, the second cell yielded the most crystalline J phase observed to date in laboratory cells. X-ray results* confirmed the metallographic examination. An FeS working electrode in a voltammetry cell was also trickle-charged potentiostatically at a voltage of 1.50 V and a temperature of 400°C for four days. Metallographic examination again showed that J phase was present. These tests indicate that (1) J phase requires a high potential for conversion to FeS, and (2) J phase is the reaction product of the second charge peak in the FeS voltammogram given in ANL-77-35, p. 58.

2. Iron Selenide Electrodes
(Z. Tomczuk)

Cell tests of various Fe(S, Se) and Fe(S, Se)$_2$ compounds are being conducted to obtain a better understanding of the chemistry and electrochemistry of the iron chalcogenides.

---

*B. S. Tani, Analytical Chemistry Laboratory.

A LiAl (2 A-hr)/LiCl-KCl/FeSe (1 A-hr) cell was operated at 433°C for 18 cycles; the best utilization was about 60%. The cell voltage was about 50 mV higher than that of a Li-Al/FeS cell, but the behavior of the FeSe cell was identical to that of FeS cells in other respects. Near the end of charge, a short, high-voltage plateau occurred at about 1.8 V in the FeSe cell; in FeS cells this plateau is attributed to conversion of J Phase ($LiK_6Fe_{24}S_{26}Cl$) to FeS. Operation of the cell was terminated after a 3-hr trickle charge to a cutoff voltage of 1.45 V. The phase found by X-ray examination* was structurally similar to J phase. The selenium compound had a cubic lattice parameter of 10.86 Å, whereas that of the sulfur compound was 10.36 Å. The selenium compound, like J phase, was insoluble in water.

3. FeS-NiS Electrode
(Z. Tomczuk, S. K. Preto, A. E. Martin)

Two LiAl (2 A-hr)/LiCl-KCl/$Fe_{0.5}Ni_{0.5}S$(1 A-hr) cells were operated to determine the effect of NiS additions on FeS cell performance (NiS and FeS were fused together prior to use in the cells). Operation of one of these cells was stopped during its first discharge. Metallographic examination and X-ray diffraction* showed that J phase, probably with nickel substituted for a portion of the iron, had formed.

The second cell was operated for 46 cycles at 460°C. The electrode utilization was only 60%, but it was constant for discharge times ranging from 3 to 9 hr. Operation of this cell was stopped at full charge (1.74 V); examinations again indicated that J phase was present. Cells of this type will probably require added current collector to achieve better utilization.

In a voltammetry experiment, an equimolar FeS-NiS electrode (75 mA-hr, capacity) yielded two, well-resolved charge and discharge peaks (beginning at 1.34 V and 1.40 V) that were nearly equal in capacity. The reactions appeared to be more reversible than those found with FeS alone (ANL-77-35, p. 57), but the utilization of the electrode was again only 60%. Future studies of the FeS-NiS electrode will be directed toward increasing its utilization and, if possible, eliminating J-phase formation.

C. Studies of Negative Electrode Properties

1. Lithium Wick Cells
(L. E. Ross)

A prismatic Li wick/FeS cell with a theoretical capacity of 70 A-hr was described earlier (ANL-77-75, p. 57). This cell short-circuited after eleven cycles because of swelling of the positive electrode. A NiS positive electrode (theoretical capacity, 51.4 A-hr) with a new, modular design (ANL-77-75, p. 57) was fabricated. Each side of this electrode consisted of three (3.4 x 6 x 0.5 cm) iron modules. The face of each module was a flat iron frame to which 40-mesh iron screens were welded. Zirconia cloth and

*B. S. Tani, Analytical Chemistry Laboratory at ANL.

325-mesh stainless steel screens were used as particle retainers, and iron Retimet served as the current collector. These modules were welded together to form an electrode that was 10.2-cm high by 6-cm wide. The lithium wick and electrolyte were the same as used in the previous cell.

This cell also failed in the eleventh cycle. In this case the short circuit was caused by excessive swelling of one of the modules followed by failure of the welds. Prior to short-circuiting, the positive utilization was 57% and the coulombic efficiency was 94%. A TiS_2 positive electrode, which may exhibit better structural stability, will be employed in the next lithium wick cell.

2. LiAl Electrodes with Additives
(D. R. Vissers, K. E. Anderson*)

Investigations are continuing (ANL-77-35, p. 52) on modifications of the Li-Al electrode that may result in sustained high capacities during extended cycling. The present studies are focused on the use of various metallic additives to the Li-Al binary alloy. The additives under investigation are indium, lead, tin, copper, zinc, magnesium, antimony, and silver.

The Li-Al-M (M=metal additives) electrodes were prepared by melting mixtures of the desired composition at about 800-900°C in tantalum crucibles. The alloy was ground to a powder and placed in an iron Retimet disk, which was enclosed in a 325-mesh stainless steel screen basket to contain the particulate material. This electrode was operated against a liquid-lithium counter electrode with the same area (15.6 cm^2) in LiCl-KCl electrolyte at ~425°C. The Li-Al-M electrodes were about 0.8 cm thick, and had theoretical capacities of approximately 10 A-hr. The relative performances of these electrodes were evaluated by comparing the capacity of the cells at various charge and discharge current densities. The data from those experiments are summarized in Table VI-1. The only additive that significantly improved capacity retention over that of an electrode with no additive was indium.

*Cell Development and Engineering Group of Chemical Engineering Division of ANL.

Table VI-1. Utilization and Capacity Retention of LiAl Electrodes with Additives

Additive	Charge Current Density, mA/cm^2	Utilization[a] at Discharge Current Density				Capacity Decline,[b] %/Cycle
		50 mA/cm^2	100 mA/cm^2	200 mA/cm^2	300 mA/cm^2	
None	50	92.3	89.2	84.6	81.9	0.06
	100	80.2	76.6	76.6	65.6	
3.9 wt % In	50	92.7	90.5	88.6	83.2	<0.01
	100	70.0	70.0	70.0	65.4	
1 wt % In	50	92.2	90.4	83.8	71.7	<0.01
	100	90.4	80.1	82.7	74.1	
5 wt % Sn	50	94.1	92.4	90.6	83.7	0.14
	100	81.9	81.9	81.9	78.4	
10 wt % Pb	50	92.2	90.2	86.2	84.2	0.30
	100	82.2	74.1	74.1	72.1	
5 wt % Cu	50	98.6	96.6	83.7	80.9	0.06
	100	66.7	65.9	65.3	63.5	
5 wt % Ag	50	94.3	93.4	91.3	88.3	0.06
	100	67.5	68.5	67.8	67.5	
5 wt % Sb	50	91.3	89.7	86.5	83.2	0.07
	100	73.4	78.3	78.3	76.7	
5 wt % Zn	50	96.5	95.0	90.6	70.2	0.06
	100	83.3	84.8	83.3	83.3	
15 wt % Mg	50	85.7	84.0	81.3	81.0	0.04
	100	61.0	58.7	58.0	57.0	

[a]Percent of theoretical lithium capacity. Data obtained during first 50 cycles.

[b]Measured at 50 mA/cm charge and discharge current densities after 200 cycles unless operation of the cell was terminated earlier.

VII. ADVANCED BATTERY RESEARCH

The objective of this work is to develop new secondary cells that use inexpensive, abundant materials. The experimental work ranges from cyclic voltammetry studies and preliminary cell tests through the construction and operation of engineering-scale cells for the most promising systems. The studies at present are focused on the development of cells having alkaline-earth negative electrodes and molten-salt electrolytes.

A. Calcium/Metal Sulfide Cells

1. Small-Scale Calcium Cells
(L. E. Ross)

Earlier studies (ANL-77-75, p. 59) were conducted on a (20 A-hr) $CaAl_2/LiCl-KCl-CaCl_2/NiS_2$ (5 A-hr) cell in which cobalt (7 wt %) was added to the positive electrode. This cell was operated at 442°C and charge and discharge cutoff voltages of 2.2 and 1.0 V, respectively. The positive electrode attained a utilization of 70% at a current density of 20 mA/cm^2 and 50% at 45 mA/cm^2.

A similar cell [(17 A-hr) $CaAl_2/LiCl-KCl-CaCl_2/NiS_2$ (4.7 A-hr)] was constructed with carbon powder (14 wt %) instead of cobalt added to the positive electrode. This cell was operated at 442°C and charge and discharge cutoff voltages of 2.2 and 0.9 V, respectively. Utilization of the positive electrode was 72% at a current density of 27 mA/cm^2, 58% at 45 mA/cm^2, and 50% at 80 mA/cm^2. These results are slightly better than those obtained with the earlier cell.

2. Large-Scale Calcium Cells
(L. E. Ross, P. Eshman,* M. F. Roche)

A $Ca(Mg_2Si)/NiS_{1.2}$ prismatic cell (90 A-hr theoretical capacity), which was started in the uncharged state, operated for 76 cycles at about 33% utilization (ANL-77-75, p. 59). After operation of the cell was terminated, it underwent metallographic examination.† This examination showed that the ZrO_2 cloth retainer on the negative electrode had been reduced to Zr_3O. Crystals of CaO, another product of the reduction, were found in the BN fabric separator. The reduction of the ZrO_2 cloth constituted an irreversible loss of cell capacity, and contributed to the low electrode utilization (33%) observed in the cell.

As a result of the above observations, another calcium cell has been put into operation. This latest cell, which has no ZrO_2 cloth on the negative electrodes, is a sealed, prismatic $Ca(Mg_2Si)/NiS_2$ cell (70 A-hr theoretical capacity) that was assembled in the uncharged state. The negative electrodes (4-mm thick) each contain Mg_2Si powder in iron Retimet current collector which is covered by a 325-mesh stainless steel screen. The positive electrode (8-mm thick) contains Ni_3S_2, CaS, and

*Industrial Cell and Battery Testing Group.

†F. C. Mrazek, Materials Development Group.

carbon fibers* (about 9 vol % of the solids in the electrode). The current collector in this electrode is a molybdenum sheet, and the electrolyte is LiCl-KCl eutectic plus 8 mol % $CaCl_2$. For the first 30 cycles, this cell achieved a specific energy of about 42 W-hr/kg at the 6-hr rate. This specific energy is 70% of the demonstration goal (60 W-hr/kg). The utilization of the theoretical capacity is about 50%, and the coulombic efficiency is 99%.

A more detailed study of the properties of the NiS_2 electrode (by cyclic voltammetry) has been initiated to define conditions that will produce higher positive electrode utilization in calcium cells. In addition, a new negative electrode (Ca_3Pb) that has a very high theoretical capacity is being studied as a possible substitute for the $Ca(Mg_2Si)$ electrode. The information developed in these studies will be used to optimize the performance of calcium/metal sulfide cells.

B. Magnesium/Metal Sulfide Cells

(C. C. Sy, Z. Tomczuk)

1. Magnesium-Lead Negative Electrodes

The properties of Mg-Pb negative electrodes for magnesium cells were studied by conducting cycling tests on two cells. Each cell contained a charged electrode (Mg-7 at. % Pb) and a discharged electrode (Mg_2Pb). These electrodes had theoretical capacities of about 12 A-hr, assuming operation between the compositions given above. The electrodes were prepared by melting the alloys into iron Retimet discs (area, 31 cm^2; thickness, 0.4 cm) at 850°C. The electrodes were separated by BN fabric. One cell contained 30 mol % NaCl-20 mol % KCl-50 mol % $MgCl_2$ electrolyte, and was operated at 450°C. The other cell contained 38 mol % LiCl-46 mol % KCl-16 mol % $MgCl_2$, and was operated at 400°C. The charge cutoff voltage and discharge cutoff voltages were +0.5 V and -0.5 V, respectively.

The cell with LiCl-KCl-$MgCl_2$ electrolyte short-circuited during its first cycle, while the cell with NaCl-KCl-$MgCl_2$ electrolyte operated for 6 cycles before developing a short circuit. During the sixth cycle the latter cell exhibited a utilization of over 90% at a current density of 30 mA/cm^2. Post-test examinations showed that the short circuit was caused by growth of magnesium dendrites through the BN fabric separator. This dendrite growth problem has also occurred with other magnesium negative electrodes (ANL-77-75, p. 59 and ANL-76-35, p. 53). Thus alloying of the magnesium is not a solution to the dendrite problem.

2. Tests of Mg/TiS_2 Cells

Two Mg_2Al_3 (5 A-hr)/TiS_2 (3 A-hr) cells were operated. One contained LiCl-KCl-$MgCl_2$ electrolyte at 410°C, and the other contained NaCl-KCl-$MgCl_2$ electrolyte at 422°C. The negative electrodes had iron housings (area, 15 cm^2; thickness, 0.4 cm), and the positive electrodes,

*Fortafil 5, Great Lakes Carbon Corp., Elizabethton, NJ, 37643.

which consisted of pressed discs of TiS_2 weighing 12 g, had carbon housings (area, 11 cm^2; thickness, 0.6 cm). Operating between cutoff voltages of 1.0 and 1.9 V, the cell with LiCl-KCl-$MgCl_2$ electrolyte exhibited a capacity of 1.57 A-hr at a current of 60 mA and 1.29 A-hr at 300 mA. The cell with LiCl-KCl-$MgCl_2$ electrolyte had a capacity of 1.96 A-hr at a current of 60 mA and 0.75 A-hr at 300 mA. Both cells had coulombic efficiencies of about 95% (a large interelectrode spacing was employed to prevent short circuits).

After operation of the cells was terminated, X-ray examination* of the discharged positive electrode from the cell with LiCl-KCl-$MgCl_2$ electrolyte showed that the reaction product was $LiTiS_2$. Formation of this product is undesirable (a magnesium-containing product is preferred) because changes in electrolyte composition occur as the cell is cycled. The product of the positive-electrode reaction in the other cell has not yet been identified. However, this cell's performance (*e.g.*, a positive-electrode utilization of only 25% at a current density of 27 mA/cm^2) is inadequate. Therefore, TiS_2 does not appear to be a satisfactory positive electrode material for magnesium cells.

3. Tests of a Mg/NiS_2 Cell

A Mg_2Al_3(20 A-hr)/LiCl-KCl-$MgCl_2$/NiS_2(7.6 A-hr) cell was operated at 423°C. The Mg_2Al_3 electrode was contained in an iron housing (area 15 cm^2; thickness, 1 cm), and the NiS_2 electrode was contained in a carbon housing (area, 11 cm^2; thickness, 0.6 cm). Carbon powder (about 3 g) was added to the NiS_2 to improve current collection. Between cutoff voltages of 1.0 and 1.9 V, the capacity of the cell was 3.1 A-hr at a current of 60 mA and 1.3 A-hr at 300 mA. (The coulombic efficiency was about 95%). The latter capacity corresponds to a positive electrode utilization of only 17% at a current density of 27 mA/cm^2.

The above magnesium-cell tests indicate that the major development problems for these cells are dendrites on negative electrodes and unacceptably low utilization in the positive electrodes. Methods of circumventing these problems will be investigated.

*B. S. Tani, Analytical Chemistry Laboratory.

REFERENCES

1. W. L. Towle, *et al.*, *Cost Estimate for the Commercial Manufacture of the Lithium/Iron Sulfide Cells for Load-Leveling*, Argonne National Laboratory Report, ANL-76-12, March 1976.

2. M. Hansen and K. Anderko, *Constitution of Binary Alloys*, McGraw-Hill, New York (1969).

APPENDIX A.

SUMMARY OF LARGE-SCALE CELL TESTS
OCTOBER-DECEMBER 1977

APPENDIX A. Summary of Large-Scale Cell Tests October-December 1977

Cell Description[a]	Max. Performance @ Indicated Rate[b] A-hr	W-hr	Rates, hr Disch.	Charge	Initial Eff.,[c] % A-hr	W-hr	Life Characteristics Days[d]	Cycles[d]	% Decline in[e] Capacity	Energy	A-hr Eff.	W-hr Eff.	Remarks
I-3-B-1, Li-Al/FeS-Cu_2S, C, S, 170/127, 13.5 x 15.6 x 3.8 cm, 2.035 kg	101 88 76 68	131 108 92 73	10 5.9 3.8 2.7	10 5.9 3.8 2.7	99	81	>326	>562	6	9	10	13	EP cell, with slightly thinner positive and slightly denser negative. 67 W-hr/kg at 10-hr rate.
I-3-B-2, Li-Al/FeS-Cu_2S C, S, 170/127, 13.5 x 15.6 x 3.8 cm, 2.07 kg	69 85	85 104	7 8.5	7 8.5	99	82	>99	>101	0	0	0	0	Previously terminated after qualification test (42 days, 48 cycles). Restarted to study cell operation at 500°C.
I-3-C-2, Li-Al/FeS-Cu_2S, C, S, 193/145, 13.5 x 15.6 x 3.8 cm (shimmed cell), 1.79 kg	97	112	10	10	98	84	>223	>429	37	34	0	4	EP cell, 4.2-mm-thick positive electrode. 63 W-hr/kg at 10-hr rate. Constant current compared to constant voltage charge. Now being tested at up to 525°C.
I-6-B-1, Li-Al/FeS_2-CoS_2, C, S, 199/156 13.5 x 15.6 x 3.2 cm, 1.61 kg	104	146	10	10	96	80	105	133	33	37	25	28	More compact EP FeS_2 cell, with thinner, less porous electrode (positive). 55 at. % Li-Al, ZrO_2 retainer cloth removed from negative electrode. 75 W-hr/kg at 4-hr rate. Terminated
I-6-B-2, Li-Al/FeS_2-CoS_2, C, S, 199/156, 13.5 x 15.6 x 3.6 cm, 1.61 kg	102	146	10	10	97	80	54	65	25	23	30	35	Similar to I-6-B-1, except Mo screen added to positive electrodes. Performance similar to I-6-B-1. Terminated
I-7-1, Li-Al/FeS_2-CoS_2, C, S, 230/222, 13.5 x 15.6 x 3.8 cm, ~1.95 kg	95	120	9.5	9.5	92	74	67	118	4	3	36	35	Compact EP one-piece positive shimmed cell. Flexible Mo connection. Tested for 4 cycles in glove box at 446°C. Terminated-poor coulombic efficiency

APPENDIX A. (Cont'd)

Cell Description[a]	Max. Performance @ Indicated Rate[b] A-hr	W-hr	Rates, hr Disch.	Charge	Initial Eff.,[c] % A-hr	W-hr	Life Characteristics Days[d]	Cycles[d]	% Decline in[e] Capacity	Energy	A-hr Eff.	W-hr Eff.	Remarks
I-8-A-1, Li-Al/FeS_2-CoS_2, C, S, 200/156, 3.5 x 15.6 x 3.2 cm, 1.72 kg	111 89	144 99	9 3.5	12 10	94	68	31	33	12	10	5	5	EP cell. Test of BN felt. Terminated after qualification test. Separator wetting problem.
I-8-A-4, Li-Al/FeS_2-CoS_2, C, S, 200/156, 13.5 x 15.6 x 3.2 cm, 1.73 kg	102	146	10	12	95	75	20	21	0	0	7	5	EP cell. Test of BN felt. 70 W-hr/kg at 4 hr-rate. Terminated after developing short circuit.
I-8-C-9, Li-Al/FeS_2-CoS_2, C, S, 200/156, 13.5 x 15.6 x 3.2 cm, 1.65 kg	110	162	10	10	89	65	1	3	0	0	0	0	EP cell. Test of BN felt. Terminated due to short circuit.
I-8-C-10, Li-Al/FeS_2-CoS_2, C, S, 200/156 13.5 x 15.6 x 3.2 cm. 1.68 kg	99	137	20	20	78	69	15	12	0	0	0	0	EP cell. Test of BN felt. Poor efficiency on initial cycles.
I-8-D-13, Li-Al/FeS_2-CoS_2, C, S, 170/156 13.5 x 15.6 x 3.8 cm, 1.95 kg	115	164	11.6	11.6	99	83	58	72	17	19	0	0	EP cell with additional Mo central plate. Terminated; poor coulombic efficiency.
I-8-F-17, Li-Al/FeS_2-CoS_2, C, S, 170/71, 13.5 x 15.6 x 3.8 cm, 1.74 kg	58	79	5.8	5.8	99	85	64	251	29	33	0	25	EP cell for study of capacity loading ratio. Terminated.
I-8-G-19, Li-Al/FeS_2-CoS_2, C, S, 75/156 13.5 x 15.6 x 3.8 cm 1.79 kg	62	95	6.2	6.2	96	78	32	85	17	18	0	0	EP cell to study capacity loading ratio. Terminated; poor capacity after temperature controller malfunction.

APPENDIX A. (Cont'd)

Cell Description[a]	Max. Performance @ Indicated Rate[b] A-hr	W-hr	Rates, hr Disch.	Charge	Initial Eff.,[c] % A-hr	W-hr	Life Characteristics Days[d]	Cycles[d]	% Decline in[e] Capacity	Energy	A-hr Eff.	W-hr Eff.	Remarks
I-8-G-20, Li-Al/FeS_2-CoS_2, C, S, 75/150 13.5 x 15.6 x 3.6 cm, 1.87 kg	40 40	61 59	4 4	4 8	97.5	78	>47	>102	0	0	0	0	EP cell. Cycling restricted to 25% of FeS_2 capacity to check lifetime effects.
I-9-3, Li-Al/FeS_2-CoS_2, C, S, 106/156, 13.5 x 15.6 x 2.61 cm, 1.38 kg	59	91	10	10	96	78	37	56	16	17	26	20	First upper-plateau cell built by EP. 60 W-hr/kg at 4-hr rate. 52 W/kg peak power. Terminated
1B4, Li-Al/FeS-Cu_2S, C, S, 146/149, 13.5 x 15.6 x 3.8 cm, 2.0 kg	84 76	98 85	10 5	10 5	86	65	>617	>998	9	8	0	0	EP thick electrode cell. Previously in series with 1B6 as Battery B7-5. Tested at 500°C (94 cycles).
G-04-009A, Li-Al/FeS_2-CoS_2, U, S, 180 UP, 14.02 x 21.0 x 3.6 cm, 2.8 kg	162	252	11	11	96	80	>5	>4	0	0	0	0	Gould, FeS_2, upper-plateau cell. Start-up.
G-04-013, Li-Al/FeS_2-CoS_2, U, S, 180 UP, 14.02 x 21.0 x 3.6 cm, 2.85 kg	122 120 118 114	197 185 163 114	25 8 4 2.5	25 8 8 8	95	69	55	68	6.8	7.5	0	0	Gould, FeS_2 upper-plateau cell. Very stable performance. Terminated to make room for next test.
G-04-013A, Li-Al/FeS_2-CoS_2, U, S, 180 UP, 14.02 x 21.0 x 3.6 cm. 2.9 kg	134	203	9	11	99	80	16	19	0	0	0	0	Gould, FeS_2 upper-plateau cell. Terminated after qualification test to make room for next cell.
G-04-025, Li-Al/FeS_2-CoS_2, U, S, 180 UP, 14.02 x 21.0 x 3.6 cm, 2.83 kg	120	179	8	8	99	77	>20	>28	0	0	0	0	Gould, FeS_2 upper-plateau cell. Qualification testing.

APPENDIX A. (Cont'd)

Cell Description[a]	Max. Performance @ Indicated Rate[b] A-hr	W-hr	Rates, hr Disch.	Charge	Initial Eff.,[c] % A-hr	W-hr	Life Characteristics Days[d]	Cycles[d]	% Decline in[e] Capacity	Energy	A-hr Eff.	W-hr Eff.	Remarks
PFC-3-01, Li-Al/FeS_2, CoS_2, C, O, 150/159 13.5 x 15.6 x 3.8 cm, 1.92 kg	109	133	10	10	98	66	44	58	34	37	8	6	First pellet cell built with no center plate in positive. Cell has high resistance thought to be due to broken Mo rod-electrode weld. Terminated.
R-31, Li-Al/NiS_2-CoS_2, U, S, 159/132, 13.3 x 15.2 x 3.5 cm, 1.88 kg	83 65	108 79	8 3.5	8 6.5	100	81	>116	>230	0	0	0	0	Four-plateau NiS_2 cell, assembled semicharged with hot-pressed NiS + Li_2S positive. Negative electrode pressed Al wire, partially charged with Li foil.
R-32, Li-Al/NiS_2, U, S, 165/127, 13.3 x 15.2 x 3.5 cm, 1.90 kg	85 65	124 79	8 3.5	8 6.5	100	80	>88	>160	0	0	2	2	Four-plateau NiS_2 cell, assembled semicharged with hot-pressed NiS + Li_2S positive. Negative electrode pressed Al wire, partially charged with Li foil.
R-33, Li-Al/NiS_2-FeS_2, U, S, 159/122, 13.3 x 15.2 x 3.5 cm, 1.90 kg	75	96	5	8	93	71	55	90	20	30	20	30	Four-plateau NiS_2-FeS_2 cell, assembled semicharged with hot-pressed NiFe + Li_2S positive. Negative electrode pressed Al wire, partially charged with Li foil. Heat-treated carbon added to the positive electrode. Terminated.
R-34, Li-Al/FeS-Cu_2S, U, S, 151/115, 13.3 x 15.2 x 3.5 cm, 2.0 kg	85	101	4	11	98	78	>21	>60	0	0	5	4	Uncharged FeS cell. Cold-pressed positive with Cu_2S and heat-treated carbon powder. Negative: pressed Al wire, partially charged with Li foil.
R-35, Li-Al/FeS_x-NiS_x-CoS_2, U, S, 144/120, 132 x 15.2 x 3.5 cm. 2.2 kg	117	177	15	16	97	81	>10	>6	0	0	0	0	Similar to R-30 except carbon fiber is added to positive electrode.

APPENDIX A. (Cont'd)

Cell Description[a]	Max. Performance @ Indicated Rate[b] A-hr	W-hr	Rates, hr Disch.	Charge	Initial Eff.,[c] % A-hr	W-hr	Life Characteristics Days[d]	Cycles[d]	% Decline in[e] Capacity	Energy	A-hr Eff.	W-hr Eff.	Remarks
VB-3, LiAl/FeS_2, U, S, 145/118, 12.7 x 12.7 x 3.2 cm, 1.85 kg	65	97	6	12	94	68	154	337	50	50	67	66	Upper-plateau, uncharged cell completely assembled in air. Negative electrode, pressed Al wire, partially charged with Li-Al plaque. Positive electrode, hot-pressed X-phase. Terminated.
M-4, LiAl/FeS_2-NiS-Mo-Fe, C, S, 165/267, 13.3 x 13.3 x 3.3 cm, 1.8 kg	135 112	187 159	9 4	9 8	99	81	>105	>170	10	21	1	5	EP cold-pressed negative/ANL hot-pressed positive. Y_2O_3 felt separator retainer. 2.7 to 3.2 mΩ cell resistance. 70 W-hr/kg at 2-hr rate.
M-5, LiAl/FeS-NiS-Fe, C, S, 139/105, 13.3 x 14.6 x 2.8 cm, 1.62 kg	73	96	7	10	97	85	83	80	16	19	41	35	FeS-NiS-Fe (S/M ~0.89) hot-pressed into current collector of Ni and Mo (no iron present). Hot-pressed negative of 55 at. % Li-Al. Y_2O_3 felt separator. 3.3-5.7 mΩ cell resistance. 59 W-hr/kg at 7-hr rate. Terminated.
KK-12, Li-Al/FeS_2-CoS_2-TiS_2, C, S, 150/95, 13.3 x 12.4 x 3.5 cm, 1.8 kg	90	126	8	10	98	81	>30	>40	0	0	0	0	Carbon-bonded FeS_2-CoS_2 positive electrode with facial TiS_2 layer (ANL) and hot-pressed LiAl (EP) electrodes. Start-up problems. Cell rebuilt with BN felt separator.
KK-13, Li-Al/NiS_2-CoS_2 C,S, 160/210, 13.3 x 13.6 x 3.6 cm, 1.7 kg	120 100	177 140	10 4	12 10	99+	82	>70	>100	6	7	0	0	Carbon-bonded Li_2S + Ni_7S_6 + CoS_2 positive and LiAl pressed + Al wire negative. Welded Mo current collector. Y_2O_3 felt separator. 78 W-hr/kg at 4-hr rate.

APPENDIX A. (Cont'd)

Cell Description[a]	Max. Performance @ Indicated Rate[b] A-hr	W-hr	Rates, hr Disch.	Charge	Initial Eff.,[c] % A-hr	W-hr	Life Characteristics Days[d]	Cycles[d]	% Decline in[e] Capacity	Energy	A-hr Eff.	W-hr Eff.	Remarks
FM-4, LiAl-5 wt % Zn/ $FeS-Cu_2S$, C, S, 85/70, 13.0 x 15.2 x 2.5 cm, 1.7 kg.	51	63	6	7	81	69	207	103	28	28	0	0	EP cold-pressed positive/ANL Li-Al-Zn in iron Retimet negative. 7.3 mΩ resistance. Terminated.
FM2-1, LiAl-8.6 wt % Sn/ $FeS_2-Co\%_2$, C, S, 86/77.5, 13.3 x 15.6 x 3.2 cm, 1.75 kg	62 61	86 93	2 5	8 8	97	74	130	255	33	34	8	3	EP cold-pressed positive/ANL Li-Al-Sn in iron Retimet negative. Upper plateau operation. Cell resistance 7.8 mΩ. Terminated.
PM-8, Li-Al/FeS, 1/2 C, S, 190/115, 13.65 x 13.02 x 4.9 cm, 2.0 kg	63	78	12.6	12.6	99	86	>70	>97	0	0	0	0	MgO powder separator, vibratory loaded. Screens & frames on positive and negative electrodes. Use of M-series cell design. No FeS additive.
PM-9, Li-Al/FeS, 1/2 C, S, 220/144, 13.65 x 13.02 x 4.2 cm, 2.0 kg	92	114	18.4	18.4	99	91	>9	>5	0	0	0	0	MgO powder separator. Hot-pressed. Screens and frames on negative only. M-series design. No FeS additive.

[a]The letters U, C, O, S, and UP are used to indicate uncharged, charged, open, sealed, and upper plateau, respectively. The capacity ratio is the number of ampere-hours in the negative electrode over the number of ampere-hours in the positive electrode. In some cases, only the capacity of the limiting electrode is given.

[b]Based on at least five cycles.

[c]Based on at least 10 cycles at the 5-hr discharge rate.

[d]The "greater than" symbols denote continuing operation.

[e]Percent decline from the maximum values at the 5-hr discharge, except where noted.

APPENDIX B.

SUMMARY OF BATTERY TESTS
OCTOBER-DECEMBER 1977

APPENDIX B. Summary of Battery Tests October-December 1977

Cell Description[a]	Max. Performance @ Indicated Rate[b] A-hr	W-hr	Rates, hr Disch.	Charge	Initial Eff.,[c] % A-hr	W-hr	Life Characteristics Days[d]	Cycles[d]	% Decline in[e] Capacity	Energy	A-hr Eff.	W-hr Eff.	Remarks
B7-S, Li-Al/FeS-Cu_2S, C, S, 149/149, 13.5 x 15.6 x 3.9 cm, 3.99 kg	100	246	10	9	99	74	491	803	40	57	19	19	Two EP thick-electrode cells in series. Total life of 1B4 is 540 days, 836 cycles; 1B6 operated for 513 days, 829 cycles. Terminated. Cell 1B6 shorted.
BB-P, Li-Al/FeS_2-CoS_2, C, S, 170/156, 13.5 x 15.6 x 3.8 cm, 6.24 kg	290	388	10	10	92	73	40	55	42	42	62	63	Three EP thick-electrode cells (I-5-4, 5, 7) in parallel. No equalization. Tests in vacuum insulated case. Testing terminated, poor coulombic efficiency.

[a]The letters U, C, O, S, and UP are used to indicate uncharged, charged, open, sealed, and upper plateau, respectively. The capacity ratio is the number of ampere-hours in the negative electrode over the number of ampere-hours in the positive electrode. In some cases, only the capacity of the limiting electrode is given.

[b]Based on at least five cycles.

[c]Based on at least 10 cycles at the 5-hr discharge rate.

[d]The "greater than" symbols denote continuing operation.

[e]Percent decline from the maximum values at the 5-hr discharge, except where noted.